

1 **Competing Atmospheric and Surface-Driven Impacts of Absorbing Aerosols**
2 **on the East Asian Summertime Climate**

3 Geeta G. Persad *

4 *Carnegie Institution for Science, Stanford, CA*

5 David J. Paynter, Yi Ming, and V. Ramaswamy

6 *NOAA/Geophysical Fluid Dynamics Laboratory, Princeton, NJ*

7 **Corresponding author address:* Geeta G. Persad, Dept. of Global Ecology, Carnegie Institution
8 for Science, 260 Panama St., Stanford , CA 94305.

9 E-mail: gpersad@carnegiescience.edu

ABSTRACT

10 East Asia has the largest concentrations of absorbing aerosols globally,
11 and these, along with the region’s scattering aerosols, have both reduced the
12 amount of solar radiation reaching the Earth’s surface regionally (“solar dim-
13 ming”) and increased shortwave absorption within the atmosphere, particu-
14 larly during the peak months of the East Asian Summer Monsoon (EASM).
15 We here analyze how atmospheric absorption and surface solar dimming com-
16 pete in driving the response of regional summertime climate to anthropogenic
17 aerosols, which dominates, and why—issues of particular importance for pre-
18 dicting how East Asian climate will respond to projected changes in absorb-
19 ing and scattering aerosol emissions in the future. We probe these questions
20 in a state-of-the-art general circulation model (GCM) using a combination
21 of realistic and novel idealized aerosol perturbations that allow us to ana-
22 lyze the relative influence of absorbing aerosols’ atmospheric and surface-
23 driven impacts on regional circulation and climate. We find that even purely
24 absorption-driven dimming decreases EASM precipitation by cooling the land
25 surface, counteracting climatological land-sea contrast and reducing ascend-
26 ing atmospheric motion and on-shore winds, despite the associated positive
27 top-of-atmosphere regional radiative forcing. Absorption-driven atmospheric
28 heating does partially offset the precipitation and surface evaporation reduc-
29 tion from its surface dimming, but the overall response to aerosol absorption
30 more closely resembles the response to its surface dimming than to its at-
31 mospheric heating. Our results provide a novel decomposition of absorbing
32 aerosol’s impacts on regional climate and demonstrate that the response can-
33 not be expected to follow the sign of absorption’s top-of-atmosphere or even
34 atmospheric radiative perturbation.

35 **1. Introduction**

36 East Asia receives over half of its annual precipitation during the summer months of June, July,
37 and August. The summertime maximum in solar radiation warms the East Asian continent more
38 rapidly than the adjacent ocean due to the land's lower heat capacity, setting up temperature and
39 pressure gradients that drive on-shore flow of moisture and ascending atmospheric motion over the
40 continent (e.g. Webster 1987). This land-sea thermal contrast, combined with orographic forcing
41 and seasonal shifts in the subtropical westerly jet, produces a precipitation maximum that peaks
42 in June and July over East Asia, known collectively as the East Asian Summer Monsoon (EASM)
43 (e.g. Murakami 1981; Chen and Bordoni 2014).

44 Superimposed on this climatological picture are changes in the radiative environment due to an-
45 thropogenic emissions over the last several decades. Aerosol concentrations over the East Asian
46 subcontinent decreased the annual mean clear-sky surface solar radiation by $4.3 \text{ W m}^{-2} \text{ decade}^{-1}$
47 from the 1960s to the 2000s (Allen et al. 2013). This “solar dimming” counteracts the climatolog-
48 ical land-sea thermal contrast by cooling the land surface more rapidly than the adjacent ocean,
49 both due to the land's lower heat capacity and because the aerosol is more strongly concentrated
50 over land than over ocean (e.g. Guo et al. 2013; Wang et al. 2015). Several modeling studies have
51 suggested that anthropogenic aerosol emissions over East Asia could be the primary contributor to
52 a weakening in EASM circulation and precipitation since the middle of the twentieth century (e.g.
53 Song et al. 2014; Wang et al. 2015), though this effect remains uncertain (Kim et al. 2016).

54 Recent work, however, has demonstrated that as much as half of the observed clear-sky reduction
55 in surface solar radiation is due to the absorption of solar radiation within the atmospheric column
56 by absorbing aerosols, as opposed to the reflection of that radiation back to space through scat-
57 tering. Persad et al. (2014) identify in general circulation model (GCM) simulations that aerosol

58 absorption under clear-sky conditions increased over East Asia by $\sim 1.6 \text{ W m}^{-2} \text{ decade}^{-1}$ from
59 the 1960s to the 2000s, robust across different model aerosol formulations. Consequently, during
60 the 2000s, the presence of anthropogenic aerosols (both scattering and absorbing) decreased East
61 Asian summertime clear-sky surface solar radiation by $\sim 20 \text{ W m}^{-2}$ and increased atmospheric
62 absorption by $\sim 10 \text{ W m}^{-2}$. This vertical radiative dipole of atmospheric heating and surface
63 dimming might be expected to have a substantially different impact on regional summertime cir-
64 culation and precipitation than surface dimming or atmospheric heating on its own, but the effects
65 of this dipole have not been cleanly decomposed before now.

66 The “semi-direct effect” of absorbing aerosols, whereby the atmospheric radiative heating from
67 direct aerosol absorption changes the thermodynamic and dynamical environment for cloud for-
68 mation, is well known (e.g. Hansen et al. 1997; Koch and Del Genio 2010). Studies show that this
69 atmospheric heating can either invigorate or suppress convection, depending on the altitude of the
70 heating relative to the climatological cloud (e.g. Johnson et al. 2004; Feingold 2005; Persad et al.
71 2012). Depending on the convective environment, atmospheric heating on its own has been shown
72 to induce strong rising atmospheric motion regionally that promotes monsoonal moisture flux and
73 convective precipitation (Chung et al. 2002; Wang 2004; Erlick et al. 2006; Meehl et al. 2008).

74 However, the same absorption process via which these aerosols heat the atmosphere also re-
75 duces the shortwave radiation at the surface, and it is unclear how these two effects will interact
76 regionally. On its own, solar dimming reduces both land surface temperature and the surface en-
77 ergy available for latent and sensible heat fluxes that help drive convection and precipitation (e.g.
78 Roeckner et al. 1999; Huang et al. 2007). In a global mean sense, solar dimming from purely-
79 scattering aerosols has been shown to spin down the hydrological cycle (Ramanathan et al. 2001).
80 Depending on the degree of coupling between the surface and atmosphere, atmospheric heating
81 from absorption may or may not be communicated to the surface and counteract the surface tem-

82 perature effects of the solar dimming (Ramanathan and Carmichael 2008). In the case of weak
83 coupling, the combination of surface cooling and atmospheric heating from aerosol absorption
84 can reduce surface-air gradients that drive evaporation, thus limiting the moisture available for
85 rainfall (Ramanathan et al. 2005).

86 Given these uncertainties and the large absorbing aerosol concentrations in East Asia, a ro-
87 bust understanding of the separate, combined, and competing effects of atmospheric heating and
88 surface dimming from aerosol absorption on the East Asian summertime climate is of crucial
89 importance, but until now has been limited. The relative effect of absorbing black carbon and
90 scattering sulfate aerosols on East Asian climate has been studied previously in a range of climate
91 models (e.g. Huang et al. 2007; Randles and Ramaswamy 2008; Guo et al. 2013; Jiang et al. 2013;
92 Wang et al. 2015). However, the total shortwave absorption due to black carbon in models and the
93 resulting ratio of surface dimming to atmospheric heating remains uncertain (Bond et al. 2013).
94 Separate analysis of surface dimming and of atmospheric heating in monsoonal systems has shown
95 substantially different impacts on regional climate (e.g. Chung et al. 2002; Roeckner et al. 1999).
96 However, the coupled effects of the two may be quite different than the sum of the parts. A holistic
97 analysis of the separate and combined impacts of surface dimming and atmospheric heating is thus
98 a crucial and missing element of a more robust understanding of absorbing aerosol impacts on the
99 EASM and East Asian summertime climate in general.

100 We here isolate and analyze the surface- vs. atmosphere-driven impacts of aerosol absorption on
101 East Asian summertime climate, using a combination of realistic and idealized forcing simulations
102 in a state-of-the-art climate model, to address the following questions. What are the competing ef-
103 fects on the EASM of increased atmospheric absorption and decreased surface solar radiation due
104 to recent regional aerosol emissions? Does the atmospheric heating from aerosol absorption en-
105 hance or counteract the circulation effects of aerosol-driven solar dimming on the EASM? Which

106 wins, and why? These are questions of interest both to present day understanding of the forcers
107 of East Asian climate variability and to our predictive ability to understand how future changes in
108 aerosol characteristics over East Asia will affect its projected regional climate.

109 **2. Methods**

110 We conduct simulations using both realistic historical aerosol emissions and idealized perturba-
111 tions in the Geophysical Fluid Dynamics Laboratory's (GFDL) AM3 Atmospheric General Cir-
112 culation Model (GCM) (Donner et al. 2011). In brief, we use a historical aerosol-only simulation
113 to derive the signal of surface dimming, atmospheric heating, and atmospheric absorption over
114 East Asia due to regional aerosol emissions. Aerosol-induced surface dimming in this model has
115 been validated against observations in Allen et al. (2013) and Persad et al. (2014), and overall
116 aerosol properties have been compared with observations in Donner et al. (2011). We then use
117 the simulated regional aerosol signal to construct a set of idealized forcing simulations in which
118 we separately impose either surface dimming, atmospheric heating, or atmospheric absorption
119 (inducing both dimming and heating) over East Asia.

120 Full details of the AM3 model may be found in Donner et al. (2011), but we here summarize
121 aspects central to this study. Crucially for this analysis, AM3 has been found to outperform other
122 models in its CMIP generation in simulating twentieth century clear-sky solar dimming over East
123 Asia (Allen et al. 2013) via a substantial contribution from aerosol absorption (Persad et al. 2014),
124 making it a reasonable tool with which to investigate the competing effects of aerosol dimming
125 and absorption on the EASM. The GFDL CM3 model suite has been previously used to study
126 East Asian summer climate as part of the CMIP5 model suite (Salzmann et al. 2014; Li et al.
127 2015). Over East Asia, AM3 exhibits relatively small biases in comparison with observations

128 in monsoon-critical parameters such as 500 mb geopotential height, surface air temperature, and
129 precipitation (Donner et al. 2011).

130 Aerosol emissions are fully interactive in AM3, i.e. prescribed aerosol emissions are transported,
131 aged, and removed according to the internal meteorology and chemistry of the model. To compute
132 radiative properties, black carbon (BC) and sulfate aerosol are assumed to be internally mixed
133 using a uniform mixing scheme, which calculates the refractive index of the mixed aerosol as the
134 volume-weighted average of BC and sulfate. All other aerosols are treated as externally mixed.
135 BC is the strongest absorber in AM3 (Ocko et al. 2012), though organic carbon is also slightly
136 absorbing in the model's formulation (Donner et al. 2011). The model contains aerosol indirect
137 effects with sulfate, sea salt, and organic carbon aerosols acting as cloud condensation nuclei
138 according to the parameterization of Ming et al. (2006) and Ming et al. (2007).

139 We first derive realistic regional aerosol effects from an ensemble of historical single forcing
140 simulations with time-varying sea surface temperature (SST) and sea ice prescribed from the
141 Hadley Centre Sea Ice and Sea Surface Temperature 1 (HADISST1) observational data set (Rayner
142 et al. 2003). The simulations are: (1) FIXED, a five-member control ensemble with all anthro-
143 pogenic emissions fixed at preindustrial (1860) values; and (2) AERO_C, a five-member ensemble
144 of experiments with historically varying anthropogenic aerosol emissions from Lamarque et al.
145 (2010) over China (as defined by national boundaries; roughly 20°–50° N and 75°–125° E), but
146 all other anthropogenic emissions (i.e. well-mixed greenhouse gases and ozone, plus all aerosol
147 emissions outside of China) fixed at preindustrial (1860) values as in FIXED. The realistic regional
148 aerosol signal, hereafter referred to as “Realistic Aerosol”, is calculated as the 1981-2000 average
149 ensemble-mean values from AERO_C minus FIXED.

150 The realistic regional aerosols absorb and scatter incoming shortwave radiation, resulting in
151 both absorption- and scattering-driven surface dimming and absorption-driven atmospheric heat-

152 ing (Section 4). We next use the aerosol radiative effects from the Realistic Aerosol signal to
 153 construct a series of idealized forcing simulations that allow us to isolate the effects of these dif-
 154 ferent components of aerosols' radiative perturbation on East Asian summertime climate. The
 155 control simulation for these is a historical simulation (ALL) with time-varying sea surface temper-
 156 ature and sea ice as in FIXED, but with all natural and anthropogenic forcings varying historically
 157 (see Donner et al. (2011) for inventories from which emissions are derived). Onto this ALL con-
 158 trol simulation, each of the three idealized perturbations described below is imposed in the years
 159 1980–2000 over Southeast China (22.5°–40° N and 100°–122.5° E)—the region of maximum
 160 aerosol emissions and radiative forcing in East Asia (Streets et al. 2013), as well as maximum cli-
 161 matological EASM precipitation. This is also the region of greatest observational coverage (Allen
 162 et al. 2013; Norris and Wild 2009; Dwyer et al. 2010) and one in which AM3's aerosol-driven so-
 163 lar dimming over East Asia has been verified against observational estimates (Persad et al. 2014).
 164 The construction and goal of each idealized forcing simulation is schematically depicted in Figure
 165 1.

166 *1. Pure Dimming:* A purely scattering optical depth (i.e. with an effective single scattering
 167 albedo of 1), scaled to reduce surface shortwave radiation by a level comparable to that produced
 168 by Realistic Aerosol, is imposed onto the ALL control. The scattering optical depth (τ_d) within
 169 each model layer of path length or depth (Δz) is calculated according to the layer average pressure
 170 (P) via the following equation, which approximates the vertical structure of the Realistic Aerosol
 perturbation:

$$\tau_d(P) = \begin{cases} \Delta z \times \alpha_d \left(\frac{P-150}{P_0} \right)^{\beta_d}, & \text{for } P \geq 150 \text{ mb} \\ 0, & \text{for } P < 150 \text{ mb} \end{cases}$$

172 where $\alpha_d = 0.117 \text{ km}^{-1}$ is a scaling constant designed to achieve a comparable magnitude of
 173 dimming as Realistic Aerosol, and $\beta_d = 2$ is a decay rate designed to approximate the vertical
 174 structure of the realistic aerosol perturbation.

175 The difference between the above perturbed simulation and the ALL simulation, averaged over
 176 1981–2000, is hereafter referred to as the “Pure Dimming” signal, and isolates the effects of sur-
 177 face dimming from that of atmospheric heating. This allows us to analyze how surface dimming
 178 from an absorber affects the overall response to the absorption, or to simulate the behavior of
 179 dimming from purely scattering aerosols.

180 *2. Pure Heating:* An idealization of the atmospheric shortwave heating profile from Realistic
 181 Aerosol is imposed onto the ALL simulation. The idealized shortwave heating rate (Tdt_{sw}) is
 182 calculated at each pressure level (P) to mimic the bottom-heavy vertical structure and magnitude
 of that produced by the realistic regional aerosol, and takes the exponential form:

$$183 \quad Tdt_{sw}(P) = \alpha_h \frac{S}{\bar{S}} \times e^{\frac{\beta_h P_0}{P}}$$

184 where $\alpha_h = 1 \text{ K s}^{-1}$ is a scaling constant designed to give a heating rate magnitude comparable to
 185 the realistic regional aerosol perturbation, and $\beta_h = 1$ is a decay rate designed to approximate the
 186 vertical structure of the realistic aerosol perturbation. The variable S is the time- and grid-varying
 187 solar flux in W m^{-2} , \bar{S} is the regionally and annually averaged solar flux in W m^{-2} , and $P_0 = 1000$
 188 mb is the surface reference pressure. The perturbation heating rate is imposed at every time step,
 189 but is scaled according to diurnal and seasonal changes in solar zenith angle and solar flux, as
 190 reflected in the $\frac{S}{\bar{S}}$ term. The resulting regional- and seasonal-mean heating rate are discussed and
 191 compared with that produced by Realistic Aerosol in Section 4c.

192 The difference between the above perturbed simulation and the ALL simulation, averaged over
 193 1981–2000, is hereafter referred to as the “Pure Heating” signal, and isolates the impact of atmo-

194 spheric heating in the absence of any associated surface dimming. In conjunction with the Pure
 195 Dimming signal, this allows us to quantify the degree to which the overall response to an aerosol
 196 population that contains absorption is influenced by its atmospheric heating versus its surface dim-
 197 ming.

198 *3. Pure Absorption:* A purely absorbing optical depth (i.e. with an effective single scattering
 199 albedo of 0) is scaled to produce surface dimming comparable to that seen in the Realistic Aerosol
 200 case. As in the Pure Dimming case, the absorbing optical depth (τ_a) within each model layer of
 201 depth (Δz) is calculated according to the layer average pressure (P) via the following equation,
 which approximates the vertical structure of the realistic regional aerosol perturbation:

$$202 \quad \tau_a(P) = \begin{cases} \Delta z \times \alpha_a \left(\frac{P-150}{P_0}\right)^{\beta_a}, & \text{for } P \geq 150 \text{ mb} \\ 0, & \text{for } P < 150 \text{ mb} \end{cases}$$

203 where $\alpha_a = 0.019 \text{ km}^{-1}$ is the magnitude scaling constant, and $\beta_a = 2$ is the vertical decay rate
 204 (identical to the Pure Dimming vertical decay rate, β_d), both designed to approximate the realistic
 205 aerosol perturbation. The resulting shortwave heating rate is compared with that produced by the
 206 Realistic Aerosol and Pure Heating cases in Section 4c.

207 The difference between the above perturbed simulation and the ALL simulation, averaged over
 208 1981–2000, is hereafter referred to as the “Pure Absorption” signal. An absorbing aerosol will both
 209 heat the atmosphere by trapping shortwave radiation therein (as in the Pure Heating simulation)
 210 and dim the surface by attenuating shortwave radiation aloft (as in the Pure Dimming simulation).
 211 This final simulation allows us to capture both effects acting in combination.

212 The Realistic Aerosol signal is primarily used to determine reasonable radiative perturbations
 213 for the idealized forcing simulations. Due to its formulation differences with the idealized forc-
 214 ing simulations, such as the presence of microphysical aerosol indirect effects in the former case

215 and differences in the control climate, precise correspondence between the Realistic Aerosol case
216 and the 3 idealized forcing signals is not expected. However, it is informative to view the Re-
217 alistic Aerosol case, which contains both scattering and absorbing aerosols, as some combina-
218 tion of the Pure Absorption and the Pure Dimming signals (with the addition of microphysical
219 aerosol indirect effects). The three idealized forcing simulations, meanwhile, are designed to
220 be more straightforwardly intercompared. Comparison of the Pure Dimming and Pure Absorp-
221 tion signals allows quantification of how the response to absorption-driven and scattering-driven
222 dimming differ. Comparison of all three idealized perturbation simulations allows the full decom-
223 position of how absorption’s atmospheric and surface radiative perturbations operate in isolation
224 and in tandem. Because of the radiative nature of the idealized perturbations’ parameterizations,
225 microphysical indirect effects—such as the Twomey (1977) and Albrecht (1989) effects—are not
226 excited directly by the idealized forcing perturbations. All cloud changes in the idealized forcing
227 simulations will thus be thermodynamically (including semi-direct aerosol effects (e.g. Hansen
228 et al. 1997)) or dynamically driven. All analysis is done on the mean of June, July, and August
229 (JJA), which captures the main Meiyu-Baiu period of EASM rainfall (e.g. Tao 1987).

230 **3. Results**

231 *a. Radiative effects of realistic and idealized aerosols*

232 Table 1 summarizes the regional-mean clear-sky and all-sky surface dimming and atmospheric
233 absorption produced by the various model perturbations, as well as their regional-mean top-of-
234 atmosphere effective radiative forcing (defined as the net downward radiative flux at the top-of-
235 the-atmosphere after atmospheric and land surface conditions have been allowed to equilibrate
236 to the perturbation (Myhre et al. 2013)). Clear-sky values are calculated by the model’s radia-

237 tive transfer code with clouds removed. Microphysical aerosol indirect effects are present in the
238 Realistic Aerosol case and may influence differences between clear-sky and all-sky (i.e. cloud-
239 permitting) values. In the idealized forcing simulations, because microphysical aerosol indirect
240 effects are not in operation, differences between all-sky and clear-sky values are explained by ei-
241 ther a) thermodynamically or dynamically driven cloud changes that reinforce or counteract the
242 aerosols' radiative interactions or b) differences due to cloud masking in the amount of radiation
243 with which the aerosol is interacting in the clear-sky versus all-sky calculation.

244 The presence of realistic regional aerosols reduces the solar radiation incident at the surface over
245 East Asia by $\Delta SSR_{all} = -14.3 \text{ W m}^{-2}$ in the 1981–2000 mean, consistent with the finding of others
246 in both models and observations (e.g. Norris and Wild 2009; Dwyer et al. 2010; Allen et al. 2013).
247 Note that, because our simulations only include aerosol emissions within China, they contain less
248 aerosol over East Asia than the models and observations in the above referenced work, which
249 include aerosols transported from both local and remote sources. The surface dimming signal is
250 evident both in the presence and in the absence of cloud cover, and is driven almost equally by
251 scattering and by absorption of shortwave radiation by aerosols within the atmospheric column
252 (consistent with the findings of Persad et al. (2014)). The similarity of the clear-sky and all-
253 sky SSR changes should not be interpreted as an absence of aerosol-cloud interactions. Aerosol
254 indirect effects operate in the Realistic Aerosol case and result in a 97% increase in cloud droplet
255 number concentration (not shown) through the activation of aerosols as cloud condensation nuclei,
256 thus increasing the shortwave cloud reflectivity (Donner et al. 2011). Simultaneously, the presence
257 of cloud above aerosol masks the interaction of the underlying scattering and absorbing aerosol
258 with downwelling shortwave radiation. With the removal of cloud in the clear-sky calculation,
259 these factors tend to compensate for one another, resulting in a net minimal difference in surface
260 shortwave radiation between the clear-sky and all-sky calculations.

261 The idealized Pure Dimming simulation—designed both to isolate the surface effects of atmo-
262 spheric absorption and to simulate the response to purely scattering-driven dimming—produces
263 an all-sky SSR reduction of $\Delta SSR_{all} = -18.6 W m^{-2}$. The difference between the clear-sky and
264 all-sky SSR reduction can be largely explained by climatological cloud-masking, as each consti-
265 tutes a comparable fractional reduction in its respective control SSR budget (10% in the clear-sky
266 case and 9% in the all-sky case). Cloud amount also decreases by approximately 3% (Table 3),
267 which appears to be consistent with the smaller all-sky SSR reduction relative to the clear-sky SSR
268 reduction. However, this is the result of a decrease in middle and high cloud and an increase in
269 low cloud, making the overall shortwave effects of the vertically integrated cloud change difficult
270 to determine.

271 Because the Pure Heating simulation—designed to isolate the atmospheric effects of aerosol
272 absorption—has a heating rate rather than an optical depth imposed, the SSR and absorption per-
273 turbations are deliberately minimal in that simulation. As evinced by the difference between the
274 clear-sky and all-sky values (Table 1), they are primarily driven by cloud changes that are consis-
275 tent with the overall circulation response discussed in Section 4c.

276 Although the absorption optical depth in the Pure Absorption case—designed to probe the
277 combined surface and atmospheric effects of purely absorption-driven dimming—is compara-
278 ble to that of the Realistic Aerosol case (see Section 2), it produces a larger amount of absorp-
279 tion due to the absence of aerosol scattering and aerosol indirect effects, which might other-
280 wise attenuate the shortwave radiation before it reaches an absorber. The increased absorption
281 ($\Delta Abs_{all} = 17.3 W m^{-2}$) produces a corresponding reduction in SSR ($\Delta SSR_{all} = -14.6 W m^{-2}$).
282 The atmospheric absorption is larger than the SSR reduction partly due to additional absorption
283 produced by shortwave radiation reflected from the surface, which is not counted in the downward-
284 incident SSR change.

285 *b. Surface energy balance response*

286 On decadal time-scales the land surface energy balance is constrained to maintain equilibrium
287 due to the low effective heat capacity of the land surface. As a result, the reduction in downwelling
288 surface shortwave flux (ΔSW_{\downarrow}) caused by the scattering and/or absorption in the 3 cases that contain
289 dimming (Realistic Aerosol, Pure Dimming, and Pure Absorption) must be compensated for by
290 changes in the other surface energy balance terms: reflected upwelling shortwave flux (ΔSW_{\uparrow}),
291 net longwave flux ($\Delta LW_{\downarrow} + \Delta LW_{\uparrow}$), sensible heat flux (ΔSH_{\uparrow}), and latent heat flux (ΔLH_{\uparrow}), i.e.
292 $\Delta F_s = (\Delta SW_{\downarrow} + \Delta SW_{\uparrow}) + (\Delta LW_{\downarrow} + \Delta LW_{\uparrow}) + \Delta SH_{\uparrow} + \Delta LH_{\uparrow} = 0$ for all values downwelling positive.

293 These changes are shown in Table 2. Slight residuals in the surface energy balance can be at-
294 tributed to the long adjustment times induced by the deep soil moisture in AM3's land model
295 (Donner et al. 2011). Surface albedo does not change significantly between the simulations, re-
296 maining at $\alpha \approx 0.16$. Consequently, the change in upwelling shortwave radiation, ΔSW_{\uparrow} , is a direct
297 result of the change in downwelling shortwave radiation, ΔSW_{\downarrow} , and $\Delta SW_{\uparrow} \approx (0.16)\Delta SW_{\downarrow}$ in all 4
298 cases. The surface upwelling longwave flux maintains a quartic relationship with surface temper-
299 ature, according to the Stefan-Boltzmann law, while sensible and latent heat flux are controlled by
300 temperature and moisture gradients between the surface and near-surface atmosphere, as well as
301 surface wind stress.

302 The idealized forcing simulations indicate that the response of the surface energy balance to
303 the reduction in SSR is dependent on the source of the dimming. When the dimming is entirely
304 scattering-driven (i.e. the Pure Dimming case), the change in latent heat flux (ΔLH_{\uparrow}) balances
305 48% of the dimming (ΔSW_{\downarrow}), while sensible heat flux (ΔSH_{\uparrow}) accounts for 28% and net longwave
306 flux ($\Delta LW_{\downarrow} + \Delta LW_{\uparrow}$) accounts for only 6.6%. Where the dimming is entirely absorption-driven (i.e.
307 the Pure Absorption case), however, the contribution from sensible heat flux exceeds that from

308 latent heat flux; reduced sensible heat flux accounts for the plurality (39%) of the surface energy
309 balance's reequilibration to the dimming, while reductions in outgoing latent heat and longwave
310 flux account for the remaining 28% and 13%, respectively. Note that upwelling shortwave flux
311 contributes the remaining energy balance equilibration in both cases, but is a simple albedo scaling
312 of the change in downwelling shortwave. Because there is not an explicit radiative perturbation
313 in the Pure Heating simulation, the perturbation to its surface energy balance cannot be construed
314 as a response to ΔSW_{\downarrow} . Indeed, radiative fluxes remain relatively unperturbed. However, outgoing
315 sensible heat flux decreases, while latent heat flux increases by a similar amount.

316 The partitioning of the surface energy balance response to dimming from Realistic Aerosol,
317 although it is driven half by atmospheric absorption (Table 1), is almost identical to the Pure
318 Dimming case. The reduction in ΔLH_{\uparrow} balances 49% of ΔSW_{\downarrow} , though ΔSH_{\uparrow} and $(\Delta LW_{\downarrow} + \Delta LW_{\uparrow})$
319 also decrease, respectively balancing 23% and 3.8% of ΔSW_{\downarrow} . This suggests that the larger sensible
320 heat flux response seen in the Pure Absorption case requires a dominating absorption contribution
321 to the dimming. We explore the mechanisms behind the relative behavior of the sensible versus
322 latent heat flux response to dimming in Section 4b.

323 *c. Impact on EASM strength*

324 As the primary mechanism for regional rainfall in East Asia, monsoon strength is frequently
325 quantified to the first order by the regional mean precipitation (e.g. Lu et al. 2006; Bollasina
326 et al. 2011). Because of their role in supporting this monsoonal precipitation, convective activity
327 and the land-sea surface temperature contrast are generally used to evaluate the overall monsoon
328 circulation strength (e.g. Wang et al. 2008; Dai et al. 2013). Consequently, we use these standard
329 parameters to characterize qualitative changes in the EASM strength: land-sea thermal contrast
330 (i.e. land surface temperature, shown in Figure 2); on-shore flow (i.e. 850 mb winds, shown

331 in Figure 3); atmospheric ascent (i.e. 500 mb vertical velocity in pressure coordinates, shown
332 in Figure 4) over land; and, ultimately, precipitation (Figure 5). We also summarize the overall
333 monsoon strength quantitatively using the total precipitation averaged over East Asia, and the 850
334 mb wind speed averaged over the East Asian monsoon sector (10° – 40° N and 110° – 150° E) as
335 defined by Li and Zeng (2002) for quantifying EASM variability (Table 3).

336 The Realistic Aerosol signal indicates that historical regional anthropogenic aerosol emissions
337 have reduced the strength of the EASM, consistent with past research (e.g. Song et al. 2014; Wang
338 et al. 2015). Although atmospheric absorption in the Realistic Aerosol case results in substantial
339 shortwave heating throughout the lower atmosphere (Section 4c), the overall radiative effects of the
340 anthropogenic aerosol loading reduces the regional-mean land surface temperature, which under
341 the fixed-SST conditions in our simulations is equivalent to a reduction in the climatological land-
342 sea thermal contrast (Fig. 2a). Decreasing land-sea contrast reduces on-shore low-level winds
343 (Fig. 3a and Table 3). The land surface cooling also drives a 6% reduction in the climatologically
344 ascending motion (i.e. $\omega_{500} < 0$) over the land surface (Fig. 4a). This overall counteraction of
345 EASM circulation causes a 6% reduction in regional-mean precipitation (Table 3 and Fig. 5a).

346 The idealized forcing simulations illuminate how the different aerosol radiative components
347 contribute to reduced EASM strength. Solar dimming from a pure scatterer (Pure Dimming)
348 decreases EASM strength by reducing the climatological land-sea thermal contrast (Fig. 2b),
349 consistent with previous studies (e.g. Guo et al. 2013; Wang et al. 2015). The deficit in surface
350 shortwave energy cools the land surface, weakening on-shore low-level winds (Fig. 3b and Table
351 3). This coincides with a 25% decrease in atmospheric ascent (Fig. 4b and Table 3) and an 8.0%
352 reduction in regional-mean precipitation (Table 3 and Fig. 5b).

353 Conversely, pure atmospheric heating in the absence of any surface shortwave perturbation (Pure
354 Heating) enhances EASM circulation in our model. The surface temperature response to the atmo-

355 spheric heating (Table 3 and Fig. 2c) is minimal. However, the imposed atmospheric shortwave
356 heating increases ascending motion over the land surface by 37% (Fig. 4c and Table 3). This
357 drives lower-level convergence that weakly increases the 850 mb flow of moisture-laden air from
358 the surrounding ocean area (Table 3 and Fig. 3c), increasing regional-mean precipitation by 6.3%
359 (Table 3 and Fig. 5c).

360 Both the solar dimming and the atmospheric heating are active in the Pure Absorption case, and
361 the EASM circulation response is correspondingly a combination of the effects of the two compo-
362 nents. While the atmospheric absorption drives an atmospheric shortwave heating rate comparable
363 to the Pure Heating case (Section 2), the attenuation of this shortwave radiation within the atmo-
364 sphere results in a substantial reduction in surface solar radiation (Table 1) that drives surface
365 cooling (Fig. 2d). The atmospheric heating enhances ascending motion by 21% (Fig. 4d and
366 Table 3), but the solar dimming simultaneously cools the land surface (Table 3). Although this
367 does reduce on-shore low-level winds (Fig. 3d), it does so by less than the Pure Dimming case
368 (Table 3). The precipitation response is small (Table 3 and Fig. 5d), but net negative (-1.6%), an
369 outcome that will be further discussed in Section 4.

370 *d. Moisture Budget Response*

371 The surface energy balance and monsoon circulation responses combine in determining the over-
372 all moisture budget response, as characterized by the response in precipitation (ΔP), evaporation
373 (ΔE , proportional to the change in surface latent heat flux), and the moisture convergence neces-
374 sary to balance the two ($\Delta(P - E)$). East Asian summertime climate is characterized by climato-
375 logical moisture convergence ($P > E$).

376 Table 4 shows the moisture budget values for each of the 4 perturbations. In the presence of
377 Realistic Aerosol or idealized Pure Dimming, P decreases by more than E and moisture conver-

378 gence decreases, consistent with the counteraction of monsoonal flow discussed in Section 3c. In
379 the Pure Heating simulation, conversely, moisture convergence increases via an increase in P that
380 is larger than the increase in E . The Pure Absorption case shows a counterbalancing of these two
381 effects; although both P and E decrease as in the Realistic Aerosol and Pure Dimming case, P
382 does so by less than E and moisture convergence consequently increases. The differences in ΔP ,
383 ΔE , and $\Delta(P - E)$ between the Pure Absorption and Pure Dimming cases (8.99, 4.81, and 4.18
384 W m^{-2} , respectively) are of the same sign as the values in the Pure Heating case and of compa-
385 rable magnitude (Table 4), suggesting that the Pure Absorption behavior can be interpreted as a
386 superposition of the Pure Dimming and Pure Heating cases. Energy balance constraints provide
387 an investigation of this outcome, discussed in Section 4a.

388 4. Discussion

389 a. *An energetic rationalization of absorption's effect on the EASM*

390 Our results demonstrate that the EASM response to realistic regional aerosol emissions is domi-
391 nated by the suppressing effect of their surface solar dimming, even in the presence of strong short-
392 wave atmospheric absorption by the aerosols. An interesting first-order question then is whether
393 the EASM response, as summarized in the regional-mean precipitation change, is at all sensitive to
394 the presence of the atmospheric absorption or is simply a response to the surface solar dimming—a
395 question that can be addressed via comparison of the results of our idealized forcing simulations.

396 Because of variations in how the imposed perturbation translates into a surface radiative effect in
397 each of our simulations (Section 2), the surface dimming values across the simulations that contain
398 an explicit radiative perturbation (i.e. Realistic Aerosol, Pure Dimming, and Pure Absorption) are
399 not identical. In order to understand how the response to a given amount of surface dimming

400 depends on the source of that dimming, we normalize out the small differences in the amount of
 401 surface dimming across our simulations to allow direct comparison. We refer to this approach as
 402 “per unit dimming” in the remainder of this work, and calculate it by dividing the response of
 403 interest (e.g. ΔP) by the change in surface shortwave radiation (ΔSSR_{all}) for a given simulation.

404 The precipitation response does not scale linearly with SSR reduction across the perturbations.
 405 The precipitation change per unit dimming in the Pure Dimming case is 3-4 times larger than that
 406 in the Pure Absorption case, indicating that the atmospheric effects of the aerosol absorption have
 407 a damping effect on the precipitation response to the surface dimming. Pure Heating on its own
 408 has little to no effect on the surface shortwave radiation or surface temperature, but increases pre-
 409 cipitation substantially, hinting at the other processes besides land-sea contrast that can influence
 410 EASM strength. The smaller precipitation reduction under Pure Absorption, thus, is not achieved
 411 via a modulation of the land-sea surface temperature contrast that drives the circulation decrease
 412 under Pure Dimming; another mechanism must be invoked.

413 We turn to the atmospheric energy and moisture budgets to seek guidance on why absorption-
 414 driven dimming would produce a smaller precipitation reduction than the same amount of purely
 415 scattering-driven dimming. The moist static energy (MSE) budget dictates that the net energy input
 416 into the atmospheric column must be balanced by the divergent moist static energy transport. In
 monsoonal systems, this balance may be approximated as follows (Chou and Neelin 2003):

$$417 \quad \left\langle \frac{\delta h}{\delta t} \right\rangle (\approx 0) = F_{net} - \langle \vec{v} \cdot \nabla h \rangle - \langle \omega \frac{\delta h}{\delta p} \rangle \quad (1)$$

418 The seasonal mean vertical integral ($\langle X \rangle$) of the time variation of moist static energy ($h = c_p T +$
 419 $gz + L_v q$, where c_p is specific heat, T is atmospheric temperature, g is gravity, z is geopotential
 420 height, L_v is the latent heat of vaporization, and q is specific humidity) can be approximated
 421 as 0, since the atmosphere’s capacity for energy storage is minimal. Thus, the net energy input

422 into the atmospheric column ($F_{net} = SW_{\uparrow}^{sfc} + SW_{\downarrow}^{sfc} + SW_{\downarrow}^{TOA} + SW_{\uparrow}^{TOA} + OLR + LW_{\downarrow}^{sfc} + LW_{\uparrow}^{sfc} +$
 423 $SH_{\uparrow} + LH_{\uparrow}$, for all values positive into the atmosphere) must be roughly balanced by the horizontal
 424 advection ($\langle \vec{v} \cdot \nabla h \rangle$) and vertical advection within the atmospheric column ($\langle \omega \frac{\delta h}{\delta p} \rangle$) of moist static
 425 energy.

426 The horizontal advection term generally can be neglected under the approximately radiative-
 427 convective equilibrium conditions of the summer monsoon (Neelin and Held 1987). Thus, equa-
 428 tion 1 can be simplified as $F_{net} \approx \langle \omega \frac{\delta h}{\delta p} \rangle$. It can be further assumed that $\langle \omega \frac{\delta h}{\delta p} \rangle < 0$ in the troposphere
 429 (e.g. Chen and Bordoni 2014), yielding the simplified proportionality: $F_{net} \propto -\langle \omega \rangle$.

430 The above relationship can then be used to understand the dynamical response to our imposed
 431 perturbations in the adjustment sense: $\Delta F_{net} \propto -\Delta \langle \omega \rangle$. Then, because the surface energy balance
 432 will rapidly equilibrate to zero over land ($\Delta F_s \approx 0$), the change in net energy input into the at-
 433 mospheric column, reduces to $\Delta F_{net} = \Delta F_s + (\Delta SW_{\downarrow}^{TOA} + \Delta SW_{\uparrow}^{TOA} + \Delta OLR) = 0 + \Delta F^{TOA}$, where
 434 ΔF^{TOA} is the change in top-of-atmosphere flux. The proportionality thus can be further approx-
 435 imated as $\Delta F^{TOA} \propto -\Delta \langle \omega \rangle$. Note that, in fixed SST simulations such as ours, the equilibrium
 436 change in top-of-atmosphere flux is equivalent to the top-of-atmosphere effective radiative forcing
 437 (ΔF^{TOA} in Table 1).

438 The proportionality, $\Delta F^{TOA} \propto -\Delta \langle \omega \rangle$, indicates that a change in the vertical integral of the
 439 vertical pressure velocity (ω) caused by an aerosol perturbation will be proportional to its TOA
 440 effective radiative forcing, i.e. a positive (negative) forcing will induce an ascending (subsiding)
 441 perturbation to vertical motion in the atmosphere. Comparison of the vertical profiles of ω (Fig.
 442 6a) and ΔF^{TOA} (Table 1) shows that this relationship holds for all 3 cases with a closed energy
 443 budget (i.e. Realistic Aerosol, Pure Dimming, and Pure Absorption), indicating that the simplified
 444 proportionality is applicable to this regime. Ascending motion must increase under Pure Absorp-
 445 tion's positive TOA forcing and decrease under Pure Scattering's negative TOA forcing.

446 Note that, because the Pure Heating case involves the artificial imposition of a shortwave heating
 447 rate, the above framework will not strictly hold, although the relative signs of $\Delta\omega$ and ΔF^{TOA}
 448 are still consistent. In this case, the imposed shortwave heating rate should be considered an
 449 additional input of energy into the atmosphere, which would need to be accounted for in the F_{net}
 450 term. Because it is artificially imposed rather than induced by an explicit radiative perturbation,
 451 unlike the shortwave heating in Pure Absorption, it is otherwise not directly reflected in the F_s or
 452 F^{TOA} terms.

453 The vertically integrated moisture budget then connects this vertical motion to the regional
 454 precipitation. To the first order, the moisture budget dictates that any change in moisture con-
 455 vergence will be proportional to the change in the integrated vertical moisture advection, i.e.
 456 $\Delta(P - E) \propto \Delta(-\langle \omega \frac{\delta q}{\delta p} \rangle)$, again assuming changes in horizontal advection are negligible under
 457 summer monsoon conditions (e.g. Chou and Neelin 2003). Changes in $\frac{\delta q}{\delta p}$ are small relative to
 458 changes in ω (Fig. 7b and Fig. 6a, respectively), so the proportionality can be approximated as
 459 $\Delta(P - E) \propto -\Delta\langle \omega \rangle$. Therefore, the enhanced ascending motion under Pure Absorption's positive
 460 ΔF^{TOA} constrains the moisture convergence to increase ($\Delta(P - E) > 0$), and the converse will be
 461 true under Pure Dimming ($\Delta(P - E) < 0$), as borne out in Table 4.

462 Both scattering- and absorption-driven surface dimming strongly suppress evaporation by de-
 463 pleting the radiative energy required to drive it ($\Delta E < 0$; Table 4), but the reduction in evaporation
 464 per unit dimming is substantially smaller under Pure Absorption than under Pure Dimming (i.e.
 465 per unit dimming $\Delta E_{PD} < \Delta E_{PA} < 0$, where PA and PD refer to the Pure Absorption and Pure
 466 Dimming cases, respectively). However, we know that moisture convergence increases under Pure
 467 Absorption ($\Delta E_{PA} < \Delta P_{PA} < 0$) and decreases under Pure Dimming ($\Delta P_{PD} < \Delta E_{PD} < 0$). Thus,
 468 the reduction in precipitation due to Pure Absorption must be smaller per unit dimming than that
 469 due to Pure Dimming ($\Delta P_{PD} < \Delta E_{PD} < \Delta E_{PA} < \Delta P_{PA} < 0$).

470 It is interesting to note that precipitation reduction per unit dimming in the Realistic Aerosol case
471 is comparable to that of the Pure Dimming case. As noted in Section 2, the Realistic Aerosol case
472 can be thought of as a combination of the Pure Dimming and Pure Absorption cases, plus aerosol
473 microphysical effects. Aerosols may suppress precipitation via microphysical indirect effects in
474 the model by reducing cloud droplet size, though this process only operates in stratiform and
475 shallow cumulus clouds in AM3's formulation (Donner et al. 2011). It is plausible, therefore, that
476 the magnitude of precipitation suppression under Realistic Aerosol should resemble that of Pure
477 Dimming, with the additional suppression from microphysical effects counteracting the reduced
478 suppression from the absorption-driven component of the realistic dimming, but direct comparison
479 is difficult for the reasons discussed in Section 2.

480 The above explanation reveals that, under the moisture convergence constraints imposed by
481 their relative top-of-atmosphere radiative forcing, the relationship between the precipitation re-
482 duction under purely absorption-driven dimming and that under purely scattering-driven dimming
483 is strongly influenced by their relative reductions in surface evaporation. Fully understanding
484 why absorption-driven dimming produces a smaller *precipitation* reduction per unit dimming than
485 scattering-driven dimming, therefore, requires an understanding of why absorption-driven dim-
486 ming produces a smaller *evaporation* reduction per unit dimming. In the next section, we ex-
487 plore the physical mechanisms behind this difference in the surface energy balance response to
488 absorption- versus scatter-driven dimming.

489 *b. Absorption's impact on surface energy flux response partitioning*

490 Aerosol-driven surface dimming over much of South and East Asia is thought to be compensated
491 for largely by a reduction in latent heat release or evaporation (Ramanathan et al. 2001, 2005), con-
492 sistent with our Realistic Aerosol case. In fully ocean-atmosphere coupled GCM runs conducted

493 by Ramanathan et al. (2005), the evaporation decrease is strongly controlled on a regional basis by
494 a reduction of the temperature and relative humidity gradient between the surface and boundary
495 layer due to dimming-driven surface cooling. This surface latent heat flux reduction can further
496 exacerbate transport-driven moisture deficits due to aerosols, such as those discussed in Section
497 3c.

498 Our idealized perturbation results, however, indicate that whether decreased surface latent or
499 sensible heat flux provides the primary balance for reduced shortwave radiation depends on the
500 degree to which that dimming is absorption-driven (Table 2); in the absence of absorption, dim-
501 ming is primarily compensated for by a latent heat flux reduction, but in the presence of absorption
502 it is primarily compensated for by a sensible heat flux reduction (Section 3b). As discussed in Sec-
503 tion 4a, this outcome helps to explain the smaller precipitation reduction under absorption-driven
504 dimming than under scattering-driven dimming. In order to understand the relative magnitude of
505 the latent heat flux reduction, we first analyze the factors controlling the behavior of the comple-
506 mentary sensible heat flux reduction.

507 Sensible heat flux can be thought of as controlled by the local gradient between surface and
508 near-surface atmospheric temperature and the wind speed. The change in horizontal wind speed
509 over land is small under all four of our perturbations (shown at 850 mb in Fig. 3), less than
510 5% of climatological values at the near-surface (10 m), so we focus here on the influence of the
511 change in the gradient between surface and near-surface air temperature ($\Delta T_s - \Delta T_a$) under purely
512 absorption-driven (Pure Absorption) versus purely scattering-driven (Pure Dimming) dimming.
513 Climatologically, the land surface is warmer than the near-surface atmosphere, encouraging the dry
514 convection of turbulent heat flux from the surface to the atmosphere. If this gradient is depressed,
515 by either land surface cooling or atmospheric warming, the surface sensible heat flux will be
516 proportionally depressed.

517 Pure Absorption can be thought of as a superposition of Pure Dimming and Pure Heating, both of
518 which exhibit a reduction in surface-to-air temperature gradient. In Pure Dimming, the depletion
519 of surface shortwave radiation cools both the surface and the near-surface atmosphere, but more
520 the surface than the atmosphere (Table 3), reducing the temperature gradient and suppressing sur-
521 face sensible heat flux (Table 2). In Pure Heating, conversely, both surface and atmosphere warm
522 (Table 3) due to the absorption-mimicking imposed shortwave heating. However, the atmosphere
523 warms by more than the surface, again reducing the temperature gradient and, consequently, re-
524 ducing surface sensible heat flux (Table 2) even in the absence of an imposed surface shortwave
525 perturbation. In the Pure Absorption case, both the surface cooling from surface shortwave deple-
526 tion and the atmospheric heating from in situ shortwave absorption are in operation. The combined
527 effects result in a larger reduction in surface-to-air temperature gradient per unit dimming than un-
528 der the Pure Dimming case (Table 3) and, consequently, stronger suppression of sensible heat flux
529 per unit dimming (Table 2 and Section 3b). Thus, surface latent heat flux need not decrease as
530 much for a given reduction in surface shortwave input as it does under the Pure Dimming condi-
531 tions. As a result, latent heat flux (i.e. evaporation) suppression is weaker under Pure Absorption
532 than under Pure Dimming, which (in combination with their relative influence on moisture con-
533 vergence) helps explain why absorption-driven dimming reduces precipitation less strongly than
534 scattering-driven dimming (Section 4a).

535 We can also use the relative changes in near-surface atmospheric temperature between Pure Ab-
536 sorption and Pure Dimming to understand the relative reduction in latent heat flux directly, though
537 it is subject to more approximating assumptions. Climatologically, for a given net surface radia-
538 tion, surface latent heat flux is controlled by the relative moisture content of the two reservoirs it
539 communicates between: the land surface and the atmosphere. Over saturated surfaces (e.g. water
540 or moist land), the surface latent heat flux is primarily determined by the near-surface atmospheric

541 water demand, generally quantified as the potential evapotranspiration (PET) (e.g. Allen et al.
542 1998). Conversely, where near-surface atmospheric water demand is greater than surface water
543 availability (e.g. arid land), variability in soil moisture is the primary controller of latent heat flux
544 from the surface to the atmosphere (e.g. Seneviratne et al. 2010). Because of the climatologically
545 high precipitation rates of the EASM, East Asian summertime latent heat flux is generally consid-
546 ered to be controlled by atmospheric water demand (e.g. Zhang et al. 2011). Thus, assuming that
547 any changes in precipitation due to the imposed perturbations will not be sufficient to change the
548 region from an atmosphere-controlled to a surface-controlled regime, the relative latent heat flux
549 response to absorption-driven versus scattering-driven dimming can be understood by analyzing
550 the relative impact of each on PET.

551 PET can be shown to be a direct function of surface air temperature, T_a , subject to various
552 simplifying assumptions (see Scheff and Frierson (2014)). The smaller decrease in T_a under
553 Pure Absorption than under Pure Dimming—a result of the balance between the atmospheric
554 absorption-induced heating and surface dimming-induced cooling—leads to a smaller decrease in
555 PET. Consequently, the near-surface atmosphere’s demand for moisture, which will be the primary
556 driver of latent heat flux under monsoon-saturated surface conditions, decreases by less per unit
557 dimming under Pure Absorption than under Pure Dimming. Given the same amount of dimming,
558 therefore, the surface shortwave flux reduction will have to be more strongly balanced by reduced
559 sensible heat flux under Pure Absorption (Section 3b), as the latent heat flux reduction will be
560 limited by the atmosphere’s relatively greater demand for moisture under Pure Absorption than
561 under Pure Dimming.

562 *c. Atmospheric processing of absorption-driven atmospheric heating*

563 The analysis in Sections 4a and 4b demonstrates the competing interplay of absorbing aerosols
564 differing surface, atmospheric, and top-of-atmosphere radiative perturbations. It is particularly
565 important to note that the sign of local surface temperature change does not correspond to the sign
566 of local TOA forcing in the case of aerosol absorption (Table 1 and 3). By depleting surface short-
567 wave radiation locally, absorbing aerosols can reduce regional surface temperatures, especially in
568 regions in which the radiative-convective coupling of the surface and atmosphere is weak (Shindell
569 and Faluvegi 2009; Ramanathan and Carmichael 2008; Bond et al. 2013). They may, however, in-
570 crease surface temperature elsewhere through tropospheric transport of their atmospheric heating
571 (Menon et al. 2002; Teng et al. 2012). Although surface-atmosphere coupling is thought to be
572 relatively strong during the EASM (Zhang et al. 2011), our results suggest that it is not sufficient
573 to overcome the cooling effects of the surface dimming.

574 If the atmospheric heating from absorption does not efficiently heat the surface, where does it
575 go? Analysis of the perturbations to various components of the atmospheric heating rates sheds
576 light on this question (Fig. 8). In the case of Pure Heating (Fig. 8b), negative dynamical heating
577 primarily compensates for the imposed shortwave atmospheric heating, indicating that the heat
578 is being transported out of the region. The dynamical heating perturbation peaks near 400 mb,
579 indicating ventilation primarily in the upper atmosphere. This completes the circulation pattern
580 indicated by the onshore flow at 850 mb and ascending motion through 500 mb (Section 3c).
581 There is weak cooling in the lower troposphere from vertical diffusion—a signal of the vertical
582 propagation of the surface sensible heat flux suppression discussed in Section 4b.

583 Under Pure Absorption (Fig. 8c), the clear-sky shortwave heating rate is similar by design to
584 that in the Pure Heating simulation, but is compensated for differently. There is some balancing

585 by dynamical cooling aloft, suggesting a similar upper atmospheric ventilation as in the Pure
586 Heating case. However, there is a larger lower atmospheric compensation by cooling from vertical
587 diffusion. This can again be attributed to vertical propagation of Pure Absorption’s larger sensible
588 heat flux suppression. Pure Dimming exhibits lower tropospheric cooling from vertical diffusion,
589 which balances lower tropospheric dynamical heating from the suppression of vertical motion
590 described in Section 4a and is consistent with the dimming-driven suppression of sensible heat flux
591 discussed in Section 4b. However, Pure Absorption’s vertical diffusional cooling is a superposition
592 of that both from Pure Heating’s atmosphere-driven sensible heat flux suppression and from Pure
593 Dimming’s dimming-driven sensible heat flux suppression, and therefore is substantially stronger,
594 as with the surface sensible heat flux suppression itself.

595 The heating rate responses to aerosol absorption’s shortwave heating demonstrate how a local
596 positive aerosol radiative forcing can coexist with negative regional surface responses through
597 transport of the heating out of the forcing region. Given the inherently regional nature of aerosol
598 forcing, due to aerosols’ short lifetime and geographically concentrated emissions sources, this
599 result demonstrates that local responses to changes in absorbing aerosol emissions should not be
600 expected to follow global-mean responses and that the surface heating effects from such changes
601 in one region may be primarily felt in other regions.

602 *d. Limitations of this work*

603 It is important to note that our study, by fixing SSTs to observations, does not incorporate
604 the potential additional EASM impacts of the ocean-mediated response to our regional pertur-
605 bations. The total regional response to aerosols can be linearly decomposed into the fast land-and-
606 atmosphere response and the slower ocean-coupled response (Hsieh et al. 2013). It is valuable,
607 therefore, to understand each part in isolation—for example, in order to understand the time evo-

608 lution of the observed response following a rapid decline in regional aerosol emissions. The radia-
609 tive forcing that the perturbations analyzed here impose in the global mean is orders of magnitude
610 smaller than what they impose at the regional level. Consequently, we would expect regional-
611 scale SST changes in the hydrological cycle to be more important than global-mean SST-mediated
612 changes (e.g. Ming et al. 2010; Samset et al. 2016) under ocean-coupled conditions.

613 Our imposed regional perturbations could modify adjacent SSTs and thus induce local ocean-
614 mediated effects on East Asian precipitation and circulation. Because our idealized forcing pertur-
615 bations are concentrated solely over land, they would only affect adjacent SSTs indirectly—e.g.
616 through circulation-induced changes in ocean surface fluxes. In the case of realistic aerosols,
617 emissions from land-based sources can be transported over the ocean (e.g. Yu et al. 2008; Wang
618 et al. 2014; Dallafior et al. 2015) where they can decrease Pacific SSTs by reducing surface short-
619 wave radiation (e.g. Boo et al. 2015; Dallafior et al. 2016), which might relax the land-sea contrast
620 induced by regional aerosols under our fixed SST conditions. We expect these ocean-mediated
621 effects to be secondary to the large direct effect that the in-situ forcing has on the land surface (e.g.
622 Hsieh et al. 2013), but their study could constitute an interesting extension of this work.

623 The complexity of the competing effects of aerosols' surface and atmospheric effects on EASM
624 strength seen in the AM3 model in our idealized forcing framework highlights the importance of
625 conducting such simulations in other model suites. The East Asian region of interest in this work is
626 one over which CMIP5 models show agreement on the sign of precipitation response to absorbing
627 aerosols, suggesting that the basic dynamics of the EASM response to absorbing aerosols is robust
628 across models (Richardson et al. 2015). However, there are several relevant absorbing aerosol
629 properties that remain a source of divergence in models (Bond et al. 2013): models disagree on the
630 simulated vertical profile of absorbing aerosols; and the efficiency with which black carbon absorb

631 shortwave radiation remains uncertain, tied particularly to variability in how models parameterize
632 mixing of different aerosol species.

633 To our knowledge, no other modeling study has separated the surface and atmospheric effects
634 of aerosol absorption over East Asia. The highly idealized nature of our forcings also precludes
635 direct comparison with observations other than that discussed in Section 2. Some other studies,
636 however, have separately simulated the effects of BC aerosol on the EASM. Such analysis can be
637 most closely compared with the results of our Pure Absorption simulation. Huang et al. (2007)
638 and Wang et al. (2015) isolate the direct effects of BC in two generations of the RegCCM regional
639 climate model over East Asia. Both studies find that summer precipitation decreases in the pres-
640 ence of BC. These studies also simulate the EASM response to all anthropogenic aerosols, and
641 comparison of the ratio of precipitation reduction to surface dimming in their BC-only versus all-
642 aerosol simulations corroborates our finding that absorption-driven dimming reduces precipitation
643 by less than scattering-driven dimming. However, the driving mechanisms behind this result are
644 not analyzed in those studies and thus cannot be compared with those discussed here.

645 **5. Conclusions**

646 The impact of absorbing aerosols on regional climate manifests through their impact both on
647 the atmospheric radiative budget and on surface energy fluxes. This work provides one of the
648 first analyses of the separate and combined effects of aerosol absorption's atmospheric and sur-
649 face perturbations on East Asian summertime climate. Our work suggests that the surface energy
650 impacts of aerosol absorption are capable of outweighing its atmospheric impacts in the net re-
651 sponse of East Asian Summer Monsoon (EASM) strength, resulting in a net decrease of EASM
652 circulation and precipitation due to the reduced land-sea contrast from dimming-induced land sur-
653 face cooling (Section 3c). Crucially, however, the precipitation reduction under absorption-driven

654 dimming is smaller per unit dimming than that under purely scattering-driven dimming, due to the
655 moisture convergence constraints imposed by their opposing signs of top-of-atmosphere radiative
656 forcing (Section 4a). This is partially influenced by stronger suppression of surface sensible heat
657 than latent heat under absorption-driven dimming and converse behavior under scattering-driven
658 dimming (Section 4b), which constrains the relative reduction in the evaporative component of
659 moisture convergence and consequently the relative reduction in the precipitation component. At-
660 mospheric heating from aerosol absorption plays a role in this additional suppression of sensible
661 heat, but it is primarily transported out of the region in the upper troposphere. Consequently, ab-
662 sorbing aerosols' impact on East Asian summertime climate more closely resemble the response
663 to its surface dimming than to its atmospheric heating.

664 The partitioning of the surface energy balance between sensible and latent heat flux (i.e. the
665 Bowen ratio, $\frac{SH}{LH}$) has myriad implications for surface temperature, convection, and boundary layer
666 depth, as well as the atmospheric moisture budget (e.g. Andrews et al. 2009). Our results indicate
667 that this partitioning is sensitive to the atmospheric forcing associated with a surface forcing:
668 absorption- and scattering-driven dimming perturb the Bowen ratio in opposite directions. We
669 provide a physical explanation here for why sensible heat suppression dominates latent heat sup-
670 pression under purely absorption-driven dimming, but the partitioning of surface energy fluxes
671 is known to be underconstrained in climate models (e.g. Dirmeyer 2011). The impact that this
672 partitioning can have on the magnitude of a precipitation response to solar dimming (Section 4a)
673 highlights the importance of better constraining this process in models.

674 This analysis sheds light on the response of East Asian summertime climate to realistic re-
675 gional aerosol emissions. Surface solar radiation reductions over this region since the 1960s have
676 been driven equally by increased aerosol scattering and increased aerosol absorption (Persad et al.
677 2014). However, the negative EASM response to historical regional aerosol emissions (Realistic

678 Aerosol)—a net reduction of onshore flow, atmospheric ascent, and regional-mean precipitation—
679 scales in proportion to purely scattering-driven dimming (Pure Dimming; Section 4a) and does
680 not exhibit the signal of absorption-driven atmospheric heating (Pure Heating), which on its own
681 invigorates EASM circulation (Section 3c). That even purely absorption-driven dimming reduces
682 EASM strength helps explain why the combined absorption- and scattering-driven dimming of
683 realistic aerosols shows such a strong EASM reduction.

684 Our idealized forcing simulations, in addition to providing physical insight on the interaction of
685 absorbing aerosols with the EASM, provide test cases at the two limits of possible future absorp-
686 tion/scattering ratios of East Asian aerosol emissions. Since 2000, scattering sulfate emissions
687 have plateaued and declined (Klimont et al. 2013; Li et al. 2013), while absorbing black carbon
688 emissions have continued to rise (Lei et al. 2011) and are expected to continue to do so at least
689 through 2030 (e.g. Levy 2009). The Pure Absorption simulation provides an extreme test case
690 of a situation in which East Asia’s aerosol concentrations are dominated by absorbing rather than
691 scattering aerosols—for example, if China continues to mitigate sulfate aerosol emissions without
692 imposing significant controls on black carbon aerosol emissions. Conversely, the Pure Dimming
693 case provides an extreme test of a scenario in which China mitigates its absorbing black carbon
694 emissions without mitigating its scattering sulfate emissions. In combination, these two simula-
695 tions suggest that increases in either aerosol type will have detrimental effects on EASM strength,
696 but that BC-driven dimming may be less detrimental than sulfate-driven dimming.

697 *Acknowledgments.* The authors thank Paul Ginoux for feedback on the early stages of this re-
698 search, and Tom Delworth and Isaac Held for helpful comments on the initial manuscript. G.
699 G. Persad was partly supported during this work by the National Science Foundation Graduate
700 Research Fellowship under grant DGE 1148900.

701 **References**

702 Albrecht, B. A., 1989: Aerosols, Cloud Microphysics, and Fractional Cloudiness. *Science*,
703 **245 (4923)**, 1227–1230, doi:10.1126/science.245.4923.1227, URL <http://science.sciencemag.org/content/245/4923/1227>.

705 Allen, R., L. S. Pereira, D. Raes, and M. Smith, 1998: Crop evapotranspiration: Guidelines for
706 computing crop water requirements. Tech. Rep. 56, Stylus, Sterling, VA.

707 Allen, R. J., J. R. Norris, and M. Wild, 2013: Evaluation of multidecadal variability in CMIP5
708 surface solar radiation and inferred underestimation of aerosol direct effects over Europe, China,
709 Japan, and India. *Journal of Geophysical Research: Atmospheres*, n/a–n/a, doi:10.1002/jgrd.
710 50426, URL <http://onlinelibrary.wiley.com/doi/10.1002/jgrd.50426/abstract>.

711 Andrews, T., P. M. Forster, and J. M. Gregory, 2009: A Surface Energy Perspective on Climate
712 Change. *Journal of Climate*, **22 (10)**, 2557–2570, doi:10.1175/2008JCLI2759.1, URL <http://journals.ametsoc.org/doi/abs/10.1175/2008JCLI2759.1>.

714 Bollasina, M. A., Y. Ming, and V. Ramaswamy, 2011: Anthropogenic Aerosols and the Weaken-
715 ing of the South Asian Summer Monsoon. *Science*, **334 (6055)**, 502–505, doi:10.1126/science.
716 1204994, URL <http://www.sciencemag.org/cgi/doi/10.1126/science.1204994>.

717 Bond, T. C., and Coauthors, 2013: Bounding the role of black carbon in the climate system: A
718 scientific assessment. *Journal of Geophysical Research: Atmospheres*, **118 (11)**, 5380–5552,
719 doi:10.1002/jgrd.50171, URL <http://doi.wiley.com/10.1002/jgrd.50171>.

720 Boo, K.-O., B. B. B. Booth, Y.-H. Byun, J. Lee, C. Cho, S. Shim, and K.-T. Kim, 2015: Influence
721 of aerosols in multidecadal SST variability simulations over the North Pacific. *Journal of Geo-*

722 *physical Research: Atmospheres*, **120** (2), 2014JD021 933, doi:10.1002/2014JD021933, URL
723 <http://onlinelibrary.wiley.com/doi/10.1002/2014JD021933/abstract>.

724 Budyko, M. I., 1963: *Evaporation Under Natural Conditions*. Israel Program for Scientific Trans-
725 lations.

726 Chen, J., and S. Bordoni, 2014: Orographic Effects of the Tibetan Plateau on the East Asian Sum-
727 mer Monsoon: An Energetic Perspective. *Journal of Climate*, **27** (8), 3052–3072, doi:10.1175/
728 JCLI-D-13-00479.1, URL <http://journals.ametsoc.org/doi/abs/10.1175/JCLI-D-13-00479.1>.

729 Chou, C., and J. D. Neelin, 2003: Mechanisms Limiting the Northward Extent
730 of the Northern Summer Monsoons over North America, Asia, and Africa*. *Jour-
731 nal of Climate*, **16** (3), 406–425, doi:10.1175/1520-0442(2003)016<0406:MLTNEO>2.
732 0.CO;2, URL [http://journals.ametsoc.org/doi/full/10.1175/1520-0442\(2003\)016%3C0406%
733 3AMLTNEO%3E2.0.CO%3B2](http://journals.ametsoc.org/doi/full/10.1175/1520-0442(2003)016%3C0406%3AMLTNEO%3E2.0.CO%3B2).

734 Chung, C. E., V. Ramanathan, and J. T. Kiehl, 2002: Effects of the south Asian absorb-
735 ing haze on the northeast monsoon and surface-air heat exchange. *Journal of climate*,
736 **15** (17), 2462–2476, URL [http://journals.ametsoc.org/doi/pdf/10.1175/1520-0442\(2002\)015%
737 3C2462%3AEOTSAA%3E2.0.CO%3B2](http://journals.ametsoc.org/doi/pdf/10.1175/1520-0442(2002)015%3C2462%3AEOTSAA%3E2.0.CO%3B2).

738 Dai, A., H. Li, Y. Sun, L.-C. Hong, L. Ho, C. Chou, and T. Zhou, 2013: The relative roles of
739 upper and lower tropospheric thermal contrasts and tropical influences in driving Asian summer
740 monsoons. *Journal of Geophysical Research: Atmospheres*, **118** (13), 7024–7045, doi:10.1002/
741 jgrd.50565, URL <http://onlinelibrary.wiley.com/doi/10.1002/jgrd.50565/abstract>.

742 Dallafior, T. N., D. Folini, R. Knutti, and M. Wild, 2015: Dimming over the oceans: Transient an-
743 thropogenic aerosol plumes in the twentieth century. *Journal of Geophysical Research: Atmo-*

744 *spheres*, **120** (8), 2014JD022 658, doi:10.1002/2014JD022658, URL <http://onlinelibrary.wiley.com/doi/10.1002/2014JD022658/abstract>.

746 Dallafior, T. N., D. Folini, R. Knutti, and M. Wild, 2016: Mixed-layer ocean responses to anthro-
747 pogenic aerosol dimming from 1870 to 2000. *Journal of Geophysical Research: Atmospheres*,
748 **121** (1), 2015JD024 070, doi:10.1002/2015JD024070, URL <http://onlinelibrary.wiley.com/doi/10.1002/2015JD024070/abstract>.

750 Dirmeyer, P. A., 2011: A History and Review of the Global Soil Wetness Project (GSWP). *Journal*
751 *of Hydrometeorology*, **12** (5), 729–749, doi:10.1175/JHM-D-10-05010.1, URL <http://journals.ametsoc.org/doi/abs/10.1175/JHM-D-10-05010.1>.

753 Donner, L. J., and Coauthors, 2011: The Dynamical Core, Physical Parameterizations, and Basic
754 Simulation Characteristics of the Atmospheric Component AM3 of the GFDL Global Coupled
755 Model CM3. *Journal of Climate*, **24** (13), 3484–3519, doi:10.1175/2011JCLI3955.1, URL <http://journals.ametsoc.org/doi/abs/10.1175/2011JCLI3955.1>.

757 Donohue, R. J., M. L. Roderick, and T. R. McVicar, 2011: Assessing the differences in sen-
758 sitivities of runoff to changes in climatic conditions across a large basin. *Journal of Hydrol-*
759 *ogy*, **406** (3–4), 234–244, doi:10.1016/j.jhydrol.2011.07.003, URL <http://www.sciencedirect.com/science/article/pii/S0022169411004306>.

761 Dwyer, J. G., J. R. Norris, and C. Ruckstuhl, 2010: Do climate models reproduce observed
762 solar dimming and brightening over China and Japan? *Journal of Geophysical Research*,
763 **115** (D7), D00K08, doi:10.1029/2009JD012945, URL <http://www.agu.org/pubs/crossref/2010/2009JD012945.shtml>.

- 765 Erlick, C., V. Ramaswamy, and L. M. Russell, 2006: Differing regional responses to a pertur-
766 bation in solar cloud absorption in the SKYHI general circulation model. *Journal of Geo-*
767 *physical Research: Atmospheres*, **111 (D6)**, D06 204, doi:10.1029/2005JD006491, URL [http:](http://onlinelibrary.wiley.com/doi/10.1029/2005JD006491/abstract)
768 [//onlinelibrary.wiley.com/doi/10.1029/2005JD006491/abstract](http://onlinelibrary.wiley.com/doi/10.1029/2005JD006491/abstract).
- 769 Feingold, G., 2005: On smoke suppression of clouds in Amazonia. *Geophysical Research*
770 *Letters*, **32 (2)**, doi:10.1029/2004GL021369, URL [http://www.agu.org/pubs/crossref/2005/](http://www.agu.org/pubs/crossref/2005/2004GL021369.shtml)
771 [2004GL021369.shtml](http://www.agu.org/pubs/crossref/2005/2004GL021369.shtml).
- 772 Fu, Q., and S. Feng, 2014: Responses of terrestrial aridity to global warming. *Journal of Geo-*
773 *physical Research: Atmospheres*, **119 (13)**, 7863–7875, doi:10.1002/2014JD021608, URL
774 <http://doi.wiley.com/10.1002/2014JD021608>.
- 775 Guo, L., E. J. Highwood, L. C. Shaffrey, and A. G. Turner, 2013: The effect of regional changes
776 in anthropogenic aerosols on rainfall of the East Asian Summer Monsoon. *Atmos. Chem. Phys.*,
777 **13 (3)**, 1521–1534, doi:10.5194/acp-13-1521-2013, URL [http://www.atmos-chem-phys.net/13/](http://www.atmos-chem-phys.net/13/1521/2013/)
778 [1521/2013/](http://www.atmos-chem-phys.net/13/1521/2013/).
- 779 Hansen, J. E., M. Sato, and R. Ruedy, 1997: Radiative Forcing and Climate Response. *Journal of*
780 *Geophysical Research*, **102 (6)**, 6831–6864.
- 781 Hsieh, W.-C., W. D. Collins, Y. Liu, J. C. H. Chiang, C.-L. Shie, K. Caldeira, and L. Cao,
782 2013: Climate response due to carbonaceous aerosols and aerosol-induced SST effects in
783 NCAR community atmospheric model CAM3.5. *Atmos. Chem. Phys.*, **13 (15)**, 7489–7510, doi:
784 [10.5194/acp-13-7489-2013](http://www.atmos-chem-phys.net/13/7489/2013/), URL <http://www.atmos-chem-phys.net/13/7489/2013/>.
- 785 Huang, Y., W. L. Chameides, and R. E. Dickinson, 2007: Direct and indirect effects of anthro-
786 pogenic aerosols on regional precipitation over east Asia. *Journal of Geophysical Research:*

787 *Atmospheres*, **112 (D3)**, D03 212, doi:10.1029/2006JD007114, URL <http://onlinelibrary.wiley.com/doi/10.1029/2006JD007114/abstract>.

789 Jiang, Y., X. Liu, X.-Q. Yang, and M. Wang, 2013: A numerical study of the effect of differ-
790 ent aerosol types on East Asian summer clouds and precipitation. *Atmospheric Environment*,
791 **70**, 51–63, doi:10.1016/j.atmosenv.2012.12.039, URL <http://www.sciencedirect.com/science/article/pii/S135223101300006X>.

793 Johnson, B., K. Shine, and P. Forster, 2004: The semi-direct aerosol effect: Impact of absorb-
794 ing aerosols on marine stratocumulus. *Quarterly Journal of the Royal Meteorological Society*,
795 **130 (599)**, 1407–1422, doi:10.1256/qj.03.61, URL <http://doi.wiley.com/10.1256/qj.03.61>.

796 Kim, M. J., S.-W. Yeh, and R. J. Park, 2016: Effects of sulfate aerosol forcing on East Asian
797 summer monsoon for 1985–2010. *Geophysical Research Letters*, **43 (3)**, 2015GL067 124,
798 doi:10.1002/2015GL067124, URL <http://onlinelibrary.wiley.com/doi/10.1002/2015GL067124/abstract>.

800 Klimont, Z., S. J. Smith, and J. Cofala, 2013: The last decade of global anthropogenic sulfur
801 dioxide: 2000–2011 emissions. *Environmental Research Letters*, **8 (1)**, 014 003, doi:10.1088/
802 1748-9326/8/1/014003, URL <http://iopscience.iop.org/1748-9326/8/1/014003>.

803 Koch, D., and A. D. Del Genio, 2010: Black carbon semi-direct effects on cloud cover: re-
804 view and synthesis. *Atmospheric Chemistry and Physics*, **10 (16)**, 7685–7696, doi:10.5194/
805 acp-10-7685-2010, URL <http://www.atmos-chem-phys.net/10/7685/2010/>.

806 Koster, R. D., and M. J. Suarez, 1999: A Simple Framework for Examining the Interannual
807 Variability of Land Surface Moisture Fluxes. *Journal of Climate*, **12 (7)**, 1911–1917, doi:

808 10.1175/1520-0442(1999)012<1911:ASFFET>2.0.CO;2, URL [http://journals.ametsoc.org/doi/abs/10.1175/1520-0442\(1999\)012%3C1911%3AASFFET%3E2.0.CO%3B2](http://journals.ametsoc.org/doi/abs/10.1175/1520-0442(1999)012%3C1911%3AASFFET%3E2.0.CO%3B2).

810 Lamarque, J.-F., and Coauthors, 2010: Historical (1850–2000) gridded anthropogenic and
811 biomass burning emissions of reactive gases and aerosols: methodology and application. *At-*
812 *mos. Chem. Phys.*, **10** (15), 7017–7039, doi:10.5194/acp-10-7017-2010, URL [http://www.](http://www.atmos-chem-phys.net/10/7017/2010/)
813 [atmos-chem-phys.net/10/7017/2010/](http://www.atmos-chem-phys.net/10/7017/2010/).

814 Lei, Y., Q. Zhang, K. B. He, and D. G. Streets, 2011: Primary anthropogenic aerosol emis-
815 sion trends for China, 1990–2005. *Atmos. Chem. Phys.*, **11** (3), 931–954, doi:10.5194/
816 [acp-11-931-2011](http://www.atmos-chem-phys.net/11/931/2011/), URL <http://www.atmos-chem-phys.net/11/931/2011/>.

817 Levy, H., 2009: *Climate Projections Based on Emissions Scenarios for Long-Lived and Short-*
818 *Lived Radiatively Active Gases and Aerosols*. DIANE Publishing.

819 Li, J., Z. Han, and Z. Xie, 2013: Model analysis of long-term trends of aerosol concentrations and
820 direct radiative forcings over East Asia. *Tellus B*, **65** (0), doi:10.3402/tellusb.v65i0.20410, URL
821 <http://www.tellusb.net/index.php/tellusb/article/view/20410>.

822 Li, J., and Q. Zeng, 2002: A unified monsoon index. *Geophysical Research Letters*, **29** (8), 115–1,
823 doi:10.1029/2001GL013874, URL [http://onlinelibrary.wiley.com/doi/10.1029/2001GL013874/](http://onlinelibrary.wiley.com/doi/10.1029/2001GL013874/abstract)
824 [abstract](http://onlinelibrary.wiley.com/doi/10.1029/2001GL013874/abstract).

825 Li, X., M. Ting, C. Li, and N. Henderson, 2015: Mechanisms of Asian Summer Monsoon
826 Changes in Response to Anthropogenic Forcing in CMIP5 Models. *Journal of Climate*,
827 **28** (10), 4107–4125, doi:10.1175/JCLI-D-14-00559.1, URL [http://journals.ametsoc.org/doi/](http://journals.ametsoc.org/doi/abs/10.1175/JCLI-D-14-00559.1)
828 [abs/10.1175/JCLI-D-14-00559.1](http://journals.ametsoc.org/doi/abs/10.1175/JCLI-D-14-00559.1).

- 829 Lu, R., B. Dong, and H. Ding, 2006: Impact of the Atlantic Multidecadal Oscillation on
830 the Asian summer monsoon. *Geophysical Research Letters*, **33** (24), L24 701, doi:10.1029/
831 2006GL027655, URL <http://onlinelibrary.wiley.com/doi/10.1029/2006GL027655/abstract>.
- 832 Meehl, G. A., J. M. Arblaster, and W. D. Collins, 2008: Effects of Black Carbon Aerosols on the
833 Indian Monsoon. *Journal of Climate*, **21** (12), 2869–2882, doi:10.1175/2007JCLI1777.1, URL
834 <http://journals.ametsoc.org/doi/abs/10.1175/2007JCLI1777.1>.
- 835 Menon, S., J. Hansen, L. Nazarenko, and Y. Luo, 2002: Climate Effects of Black Carbon Aerosols
836 in China and India. *Science*, **297** (5590), 2250–2253, doi:10.1126/science.1075159, URL <http://www.sciencemag.org/content/297/5590/2250>.
- 838 Milly, P. C. D., 1994: Climate, soil water storage, and the average annual water balance. *Water*
839 *Resources Research*, **30** (7), 2143–2156, doi:10.1029/94WR00586, URL <http://onlinelibrary.wiley.com/doi/10.1029/94WR00586/abstract>.
- 841 Ming, Y., V. Ramaswamy, L. J. Donner, and V. T. Phillips, 2006: A new parameterization of cloud
842 droplet activation applicable to general circulation models. *Journal of the atmospheric sciences*,
843 **63** (4), 1348–1356, URL <http://journals.ametsoc.org/doi/abs/10.1175/JAS3686.1>.
- 844 Ming, Y., V. Ramaswamy, L. J. Donner, V. T. J. Phillips, S. A. Klein, P. A. Ginoux, and L. W.
845 Horowitz, 2007: Modeling the Interactions between Aerosols and Liquid Water Clouds with
846 a Self-Consistent Cloud Scheme in a General Circulation Model. *Journal of the Atmospheric*
847 *Sciences*, **64** (4), 1189–1209, doi:10.1175/JAS3874.1, URL <http://journals.ametsoc.org/doi/abs/10.1175/JAS3874.1>.
- 849 Ming, Y., V. Ramaswamy, and G. Persad, 2010: Two Opposing Effects of Absorbing
850 Aerosols on Global-Mean Precipitation. *Geophysical Research Letters*, **37** (13), doi:10.1029/

851 2010GL042895.

852 Murakami, T., 1981: Orographic Influence of the Tibetan Plateau on the Asiatic Winter Monsoon
853 Circulation Part 1: Large-Scale Aspects. *Journal of the Meteorological Society of Japan. Ser. II*,
854 **59 (1)**, 40–65.

855 Myhre, G., and Coauthors, 2013: Anthropogenic and Natural Radiative Forcing. *Climate Change*
856 *2013: The Physical Science Basis. Contribution of Working Group I to the Fifth Assessment*
857 *Report of the Intergovernmental Panel on Climate Change*, T. F. Stocker, D. Qin, G.-K. Plattner,
858 M. Tignor, S. Allen, J. Boschung, A. Nauels, Y. Xia, V. Bex, and P. Midgley, Eds., Cambridge
859 University Press, Cambridge, United Kingdom and New York, NY, USA.

860 Neelin, J. D., and I. M. Held, 1987: Modeling Tropical Convergence Based on the Moist Static En-
861 ergy Budget. *Monthly Weather Review*, **115 (1)**, 3–12, doi:10.1175/1520-0493(1987)115<0003:
862 MTCBOT>2.0.CO;2, URL [http://journals.ametsoc.org/doi/abs/10.1175/1520-0493\(1987\)115%](http://journals.ametsoc.org/doi/abs/10.1175/1520-0493(1987)115%3C0003:MTCBOT%3E2.0.CO;2)
863 [3C0003:MTCBOT%3E2.0.CO;2](http://journals.ametsoc.org/doi/abs/10.1175/1520-0493(1987)115%3C0003:MTCBOT%3E2.0.CO;2).

864 Norris, J. R., and M. Wild, 2009: Trends in aerosol radiative effects over China and Japan in-
865 ferred from observed cloud cover, solar “dimming,” and solar “brightening”. *Journal of Geo-*
866 *physical Research*, **114 (D10)**, D00D15, doi:10.1029/2008JD011378, URL [http://www.agu.org/](http://www.agu.org/pubs/crossref/2009/2008JD011378.shtml)
867 [pubs/crossref/2009/2008JD011378.shtml](http://www.agu.org/pubs/crossref/2009/2008JD011378.shtml).

868 Ocko, I. B., V. Ramaswamy, P. Ginoux, Y. Ming, and L. W. Horowitz, 2012: Sensitivity of scat-
869 tering and absorbing aerosol direct radiative forcing to physical climate factors. *Journal of*
870 *Geophysical Research: Atmospheres*, **117 (D20)**, n/a–n/a, doi:10.1029/2012JD018019, URL
871 <http://onlinelibrary.wiley.com/doi/10.1029/2012JD018019/abstract>.

- 872 Persad, G. G., Y. Ming, and V. Ramaswamy, 2012: Tropical Tropospheric-Only Responses to
873 Absorbing Aerosols. *Journal of Climate*, **25** (7), 2471–2480, doi:10.1175/JCLI-D-11-00122.1,
874 URL <http://journals.ametsoc.org/doi/abs/10.1175/JCLI-D-11-00122.1>.
- 875 Persad, G. G., Y. Ming, and V. Ramaswamy, 2014: The role of aerosol absorption in driving clear-
876 sky solar dimming over East Asia. *Journal of Geophysical Research: Atmospheres*, n/a–n/a,
877 doi:10.1002/2014JD021577, URL [http://onlinelibrary.wiley.com/doi/10.1002/2014JD021577/](http://onlinelibrary.wiley.com/doi/10.1002/2014JD021577/abstract)
878 abstract.
- 879 Ramanathan, V., and G. Carmichael, 2008: Global and regional climate changes due to black
880 carbon. *Nature Geoscience*, **1** (4), 221–227, URL [http://www.nature.com/ngeo/journal/vaop/](http://www.nature.com/ngeo/journal/vaop/ncurrent/full/ngeo156.html)
881 ncurrent/full/ngeo156.html.
- 882 Ramanathan, V., P. J. Crutzen, J. T. Kiehl, and D. Rosenfeld, 2001: Aerosols, Climate, and the
883 Hydrological Cycle. *Science*, **294** (5549), 2119–2124, doi:10.1126/science.1064034, URL <http://www.sciencemag.org/content/294/5549/2119>.
884
- 885 Ramanathan, V., and Coauthors, 2005: Atmospheric brown clouds: Impacts on South Asian cli-
886 mate and hydrological cycle. *Proceedings of the National Academy of Sciences of the United*
887 *States of America*, **102** (15), 5326–5333, doi:10.1073/pnas.0500656102, URL [http://www.pnas.](http://www.pnas.org/content/102/15/5326)
888 org/content/102/15/5326.
- 889 Randles, C. A., and V. Ramaswamy, 2008: Absorbing aerosols over Asia: A Geophysical
890 Fluid Dynamics Laboratory general circulation model sensitivity study of model response to
891 aerosol optical depth and aerosol absorption. *Journal of Geophysical Research: Atmospheres*,
892 **113** (D21), D21 203, doi:10.1029/2008JD010140, URL [http://onlinelibrary.wiley.com/doi/10.](http://onlinelibrary.wiley.com/doi/10.1029/2008JD010140/abstract)
893 1029/2008JD010140/abstract.

- 894 Rayner, N. A., D. E. Parker, E. B. Horton, C. K. Folland, L. V. Alexander, D. P. Rowell, E. C.
895 Kent, and A. Kaplan, 2003: Global analyses of sea surface temperature, sea ice, and night ma-
896 rine air temperature since the late nineteenth century. *Journal of Geophysical Research: Atmo-*
897 *spheres*, **108 (D14)**, n/a–n/a, doi:10.1029/2002JD002670, URL [http://onlinelibrary.wiley.com/](http://onlinelibrary.wiley.com/doi/10.1029/2002JD002670/abstract)
898 [doi/10.1029/2002JD002670/abstract](http://onlinelibrary.wiley.com/doi/10.1029/2002JD002670/abstract).
- 899 Richardson, T. B., P. M. Forster, T. Andrews, and D. J. Parker, 2015: Understanding the Rapid
900 Precipitation Response to CO₂ and Aerosol Forcing on a Regional Scale. *Journal of Climate*,
901 **29 (2)**, 583–594, doi:10.1175/JCLI-D-15-0174.1, URL [http://journals.ametsoc.org/doi/abs/10.](http://journals.ametsoc.org/doi/abs/10.1175/JCLI-D-15-0174.1)
902 [1175/JCLI-D-15-0174.1](http://journals.ametsoc.org/doi/abs/10.1175/JCLI-D-15-0174.1).
- 903 Roeckner, E., L. Bengtsson, J. Feichter, J. Lelieveld, and H. Rodhe, 1999: Transient Climate
904 Change Simulations with a Coupled Atmosphere–Ocean GCM Including the Tropospheric Sul-
905 fur Cycle. *Journal of Climate*, **12 (10)**, 3004–3032, doi:10.1175/1520-0442(1999)012<3004:
906 TCCSWA>2.0.CO;2, URL [http://journals.ametsoc.org/doi/abs/10.1175/1520-0442%281999%](http://journals.ametsoc.org/doi/abs/10.1175/1520-0442%281999%29012%3C3004%3ATCCSWA%3E2.0.CO%3B2)
907 [29012%3C3004%3ATCCSWA%3E2.0.CO%3B2](http://journals.ametsoc.org/doi/abs/10.1175/1520-0442%281999%29012%3C3004%3ATCCSWA%3E2.0.CO%3B2).
- 908 Salzmänn, M., H. Weser, and R. Cherian, 2014: Robust response of Asian summer monsoon
909 to anthropogenic aerosols in CMIP5 models. *Journal of Geophysical Research: Atmospheres*,
910 **119 (19)**, 11,321–11,337, doi:10.1002/2014JD021783, URL [http://onlinelibrary.wiley.com/doi/](http://onlinelibrary.wiley.com/doi/10.1002/2014JD021783/abstract)
911 [10.1002/2014JD021783/abstract](http://onlinelibrary.wiley.com/doi/10.1002/2014JD021783/abstract).
- 912 Samset, B. H., and Coauthors, 2016: Fast and slow precipitation responses to individual climate
913 forcers: A PDRMIP multimodel study. *Geophysical Research Letters*, **43 (6)**, 2016GL068064,
914 doi:10.1002/2016GL068064, URL [http://onlinelibrary.wiley.com/doi/10.1002/2016GL068064/](http://onlinelibrary.wiley.com/doi/10.1002/2016GL068064/abstract)
915 [abstract](http://onlinelibrary.wiley.com/doi/10.1002/2016GL068064/abstract).

916 Scheff, J., and D. M. W. Frierson, 2014: Scaling Potential Evapotranspiration with Greenhouse
917 Warming. *Journal of Climate*, **27** (4), 1539–1558, doi:10.1175/JCLI-D-13-00233.1, URL <http://journals.ametsoc.org/doi/abs/10.1175/JCLI-D-13-00233.1>.
918

919 Scheff, J., and D. M. W. Frierson, 2015: Terrestrial Aridity and Its Response to Greenhouse
920 Warming across CMIP5 Climate Models. *Journal of Climate*, **28** (14), 5583–5600, doi:10.1175/
921 JCLI-D-14-00480.1, URL <http://journals.ametsoc.org/doi/abs/10.1175/JCLI-D-14-00480.1>.

922 Seneviratne, S. I., T. Corti, E. L. Davin, M. Hirschi, E. B. Jaeger, I. Lehner, B. Orlowsky, and
923 A. J. Teuling, 2010: Investigating soil moisture–climate interactions in a changing climate: A
924 review. *Earth-Science Reviews*, **99** (3–4), 125–161, doi:10.1016/j.earscirev.2010.02.004, URL
925 <http://www.sciencedirect.com/science/article/pii/S0012825210000139>.

926 Shindell, D., and G. Faluvegi, 2009: Climate response to regional radiative forcing during the
927 twentieth century. *Nature Geoscience*, **2** (4), 294–300, doi:10.1038/ngeo473, URL <http://www.nature.com/ngeo/journal/v2/n4/abs/ngeo473.html>.
928

929 Song, F., T. Zhou, and Y. Qian, 2014: Responses of East Asian summer monsoon to natu-
930 ral and anthropogenic forcings in the 17 latest CMIP5 models. *Geophysical Research Let-
931 ters*, **41** (2), 596–603, doi:10.1002/2013GL058705, URL [http://onlinelibrary.wiley.com/doi/10.
932 1002/2013GL058705/abstract](http://onlinelibrary.wiley.com/doi/10.1002/2013GL058705/abstract).

933 Streets, D. G., D. T. Shindell, Z. Lu, and G. Faluvegi, 2013: Radiative forcing due to major aerosol
934 emitting sectors in China and India. *Geophysical Research Letters*, n/a–n/a, doi:10.1002/grl.
935 50805, URL <http://onlinelibrary.wiley.com/doi/10.1002/grl.50805/abstract>.

936 Tao, S. Y., 1987: A review of recent research on the East Asian summer monsoon in China.
937 *Monsoon Meteorology*, T. N. K. C. P. Chang, Ed., Oxford University Press, 60–92, URL <http://>

938 //ci.nii.ac.jp/naid/10013126169/.

939 Teng, H., W. M. Washington, G. Branstator, G. A. Meehl, and J.-F. Lamarque, 2012: Poten-
940 tial impacts of Asian carbon aerosols on future US warming. *Geophysical Research Letters*,
941 **39** (11), n/a–n/a, doi:10.1029/2012GL051723, URL [http://onlinelibrary.wiley.com/doi/10.1029/](http://onlinelibrary.wiley.com/doi/10.1029/2012GL051723/abstract)
942 2012GL051723/abstract.

943 Twomey, S., 1977: The Influence of Pollution on the Shortwave Albedo of Clouds. *Jour-*
944 *nal of the Atmospheric Sciences*, **34** (7), 1149–1152, doi:10.1175/1520-0469(1977)034<1149:
945 TIOPOT>2.0.CO;2, URL [http://journals.ametsoc.org/doi/abs/10.1175/1520-0469%281977%](http://journals.ametsoc.org/doi/abs/10.1175/1520-0469%281977%29034%3C1149%3ATIOPOT%3E2.0.CO%3B2)
946 29034%3C1149%3ATIOPOT%3E2.0.CO%3B2.

947 Wang, B., Z. Wu, J. Li, J. Liu, C.-P. Chang, Y. Ding, and G. Wu, 2008: How to Measure the
948 Strength of the East Asian Summer Monsoon. *Journal of Climate*, **21** (17), 4449–4463, doi:
949 10.1175/2008JCLI2183.1, URL <http://journals.ametsoc.org/doi/abs/10.1175/2008JCLI2183.1>.

950 Wang, C., 2004: A modeling study on the climate impacts of black carbon aerosols. *Journal of*
951 *Geophysical Research: Atmospheres*, **109** (D3), D03 106, doi:10.1029/2003JD004084, URL
952 <http://onlinelibrary.wiley.com/doi/10.1029/2003JD004084/abstract>.

953 Wang, T. J., and Coauthors, 2015: The interactions between anthropogenic aerosols and the East
954 Asian summer monsoon using RegCCMS. *Journal of Geophysical Research: Atmospheres*,
955 2014JD022877, doi:10.1002/2014JD022877, URL [http://onlinelibrary.wiley.com/doi/10.1002/](http://onlinelibrary.wiley.com/doi/10.1002/2014JD022877/abstract)
956 2014JD022877/abstract.

957 Wang, Y., and Coauthors, 2014: Assessing the effects of anthropogenic aerosols on Pacific storm
958 track using a multiscale global climate model. *Proceedings of the National Academy of Sciences*,

959 **111 (19)**, 6894–6899, doi:10.1073/pnas.1403364111, URL <http://www.pnas.org/content/111/>
960 [19/6894](http://www.pnas.org/content/111/19/6894).

961 Webster, P., 1987: The elementary monsoon. *Monsoons*, J.S. Fein and P.L. Stephens, Eds., John
962 Wiley and Sons, 3–32.

963 Yu, H., L. A. Remer, M. Chin, H. Bian, R. G. Kleidman, and T. Diehl, 2008: A satellite-based
964 assessment of transpacific transport of pollution aerosol. *Journal of Geophysical Research: At-*
965 *mospheres*, **113 (D14)**, D14S12, doi:10.1029/2007JD009349, URL [http://onlinelibrary.wiley.](http://onlinelibrary.wiley.com/doi/10.1029/2007JD009349/abstract)
966 [com/doi/10.1029/2007JD009349/abstract](http://onlinelibrary.wiley.com/doi/10.1029/2007JD009349/abstract).

967 Zhang, J., L. Wu, and W. Dong, 2011: Land-atmosphere coupling and summer climate variability
968 over East Asia. *Journal of Geophysical Research: Atmospheres*, **116 (D5)**, D05 117, doi:10.
969 [1029/2010JD014714](http://onlinelibrary.wiley.com/doi/10.1029/2010JD014714), URL <http://onlinelibrary.wiley.com/doi/10.1029/2010JD014714/abstract>.

970 **LIST OF TABLES**

971 **Table 1.** Regional-mean radiative perturbations over East Asia (22.5°–40° N; 100°–
972 122.5° E) are shown for each of the 4 simulations. The changes in all-sky
973 (ΔSSR_{all}) and clear-sky (ΔSSR_{clr}) surface shortwave radiation, all-sky (ΔAbs_{all})
974 and clear-sky (ΔAbs_{clr}) atmospheric shortwave absorption, and regional all-sky
975 (ΔF_{all}^{TOA}) and clear-sky (ΔF_{clr}^{TOA}) top-of-atmosphere effective radiative forcing
976 are in $W m^{-2}$. Asterisks indicate perturbations that are not significant at the
977 95% confidence level. 47

978 **Table 2.** Regional-mean surface energy flux changes over East Asia (22.5°–40° N;
979 100°–122.5° E) are shown for each of the 4 simulations in units of $W m^{-2}$,
980 as well as the residual of all surface energy balance adjustment. All values
981 are given as downward positive. Asterisks indicate perturbations that are not
982 significant at the 95% confidence level. 48

983 **Table 3.** Regional-mean responses over East Asia (22.5°–40° N; 100°–122.5° E) are
984 shown for each of the 4 perturbations. The change in column integrated cloud
985 amount ($\Delta Cloud$) is given in percent of grid cloud coverage, the change in
986 surface (ΔT_s) and near-surface air (ΔT_a) temperature is given in degrees Kelvin,
987 the change in precipitation ($\Delta P/P$) is given in percent of climatological values,
988 and the change in vertical pressure velocity at 500 mb ($\Delta \omega_{500}$) is given in 10^{-3}
989 $Pa s^{-1}$. The change in 850 mb wind speed (ΔV_{850}) is averaged over the East
990 Asian monsoon sector (10°–40° N; 110°–150° E) following Li and Zeng (2002).
991 Asterisks indicate perturbations that are not significant at the 95% confidence
992 level. 49

993 **Table 4.** The moisture budget averaged over East Asia (22.5°–40° N; 100°–122.5° E) is
994 shown for each of the 4 perturbations. Changes in precipitation (ΔP), evapora-
995 tion (ΔE , cf. Δ Latent Heat in Table 2), and moisture convergence ($\Delta(P - E)$)
996 values are given in units of $W m^{-2}$ 50

997 TABLE 1. Regional-mean radiative perturbations over East Asia (22.5°–40° N; 100°–122.5° E) are shown for
 998 each of the 4 simulations. The changes in all-sky (ΔSSR_{all}) and clear-sky (ΔSSR_{clr}) surface shortwave radiation,
 999 all-sky (ΔAbs_{all}) and clear-sky (ΔAbs_{clr}) atmospheric shortwave absorption, and regional all-sky (ΔF_{all}^{TOA}) and
 1000 clear-sky (ΔF_{clr}^{TOA}) top-of-atmosphere effective radiative forcing are in $W\ m^{-2}$. Asterisks indicate perturbations
 1001 that are not significant at the 95% confidence level.

	Realistic Aerosol	Pure Dimming	Pure Heating	Pure Absorption
ΔSSR_{all}	-14.3	-18.6	-0.19*	-14.6
ΔSSR_{clr}	-13.5	-29.0	0.04*	-16.2
ΔAbs_{all}	6.87	-1.35	-0.49*	17.3
ΔAbs_{clr}	7.29	-2.76	0.10*	19.1
ΔF_{all}^{TOA}	-6.75	-19.8	2.04*	6.57
ΔF_{clr}^{TOA}	-4.35	-27.4	0.09*	6.13

1002 TABLE 2. Regional-mean surface energy flux changes over East Asia (22.5°–40° N; 100°–122.5° E) are
 1003 shown for each of the 4 simulations in units of $W m^{-2}$, as well as the residual of all surface energy balance
 1004 adjustment. All values are given as downward positive. Asterisks indicate perturbations that are not significant
 1005 at the 95% confidence level.

	Realistic Aerosol	Pure Dimming	Pure Heating	Pure Absorption
ΔSW_{\downarrow}	-14.3	-18.6	-0.19*	-14.6
ΔSW_{\uparrow}	2.09	2.64	0.03*	2.37
ΔLW_{\downarrow}	-0.62	-3.22	-0.12*	-0.43*
ΔLW_{\uparrow}	1.16	4.45	-0.09*	2.36
ΔSH_{\uparrow}	3.23	5.30	2.00*	5.71
ΔLH_{\uparrow}	7.13	8.95	-1.82	4.14
<i>Residual</i>	-1.31	-0.48	-0.19	-0.45

1006 TABLE 3. Regional-mean responses over East Asia (22.5°–40° N; 100°–122.5° E) are shown for each of
 1007 the 4 perturbations. The change in column integrated cloud amount (ΔCloud) is given in percent of grid cloud
 1008 coverage, the change in surface (ΔT_s) and near-surface air (ΔT_a) temperature is given in degrees Kelvin, the
 1009 change in precipitation ($\Delta P/P$) is given in percent of climatological values, and the change in vertical pressure
 1010 velocity at 500 mb ($\Delta\omega_{500}$) is given in $10^{-3} \text{ Pa s}^{-1}$. The change in 850 mb wind speed (ΔV_{850}) is averaged
 1011 over the East Asian monsoon sector (10°–40° N; 110°–150° E) following Li and Zeng (2002). Asterisks indicate
 1012 perturbations that are not significant at the 95% confidence level.

	Realistic Aerosol	Pure Dimming	Pure Heating	Pure Absorption
ΔCloud	-0.28*	-0.87	0.41	1.14
ΔT_s	-0.18	-0.74	0.01*	-0.38
ΔT_a	-0.08	-0.69	0.04	-0.33
$\Delta P/P$	-6.0	-8.0	6.3	-1.6
$\Delta\omega_{500}$	1.0	3.5	-5.2	-3.0
ΔV_{850}	-0.01*	-0.11	0.04*	-0.08

1013 TABLE 4. The moisture budget averaged over East Asia (22.5°–40° N; 100°–122.5° E) is shown for each of
 1014 the 4 perturbations. Changes in precipitation (ΔP), evaporation (ΔE , cf. Δ Latent Heat in Table 2), and moisture
 1015 convergence ($\Delta(P - E)$) values are given in units of W m^{-2} .

	Realistic Aerosol	Pure Dimming	Pure Heating	Pure Absorption
ΔP	-9.35	-11.17	8.77	-2.18
ΔE	-7.13	-8.95	1.82	-4.14
$\Delta(P - E)$	-2.22	-2.22	6.95	1.96

1016 **LIST OF FIGURES**

1017 **Fig. 1.** The 3 idealized forcing perturbations are schematically depicted. Each of the depicted per-
 1018 turbations is imposed over Southeast China (22.5°–40° N and 100°–122.5° E) during years
 1019 1980–2000 of an ALL control simulation, which contains historically varying anthropogenic
 1020 and natural emissions and observationally prescribed sea surface temperature and sea ice. . . . 52

1021 **Fig. 2.** The surface temperature response (shading; in K) to (a) historical regional aerosols, (b) a
 1022 purely scattering aerosol optical depth, (c) idealized atmospheric heating, and (d) a purely
 1023 absorbing aerosol optical depth. Climatological values are shown in grey contours, and
 1024 coastal outlines are shown in black. The red box delineates East Asia (22.5°–40° N; 100°–
 1025 122.5° E), over which idealized perturbations are imposed and regional-means are calcu-
 1026 lated. Stippling indicates responses that are significant at the 95% confidence level. . . . 53

1027 **Fig. 3.** The change in 850 mb wind velocity (vectors; in m s^{-1}) in response to (a) historical re-
 1028 gional aerosols, (b) a purely scattering aerosol optical depth, (c) idealized atmospheric heat-
 1029 ing, and (d) a purely absorbing aerosol optical depth. Wind vectors are only shown for
 1030 changes that are significant at the 95% confidence level. Climatological wind speeds (in m s^{-1})
 1031 are shaded, with sign convention following meridional wind direction (southerly posi-
 1032 tive). Coastal outlines are shown in black. The red box delineates East Asia (22.5°–40°
 1033 N; 100°–122.5° E), over which idealized perturbations are imposed and regional-means are
 1034 calculated. . . . 54

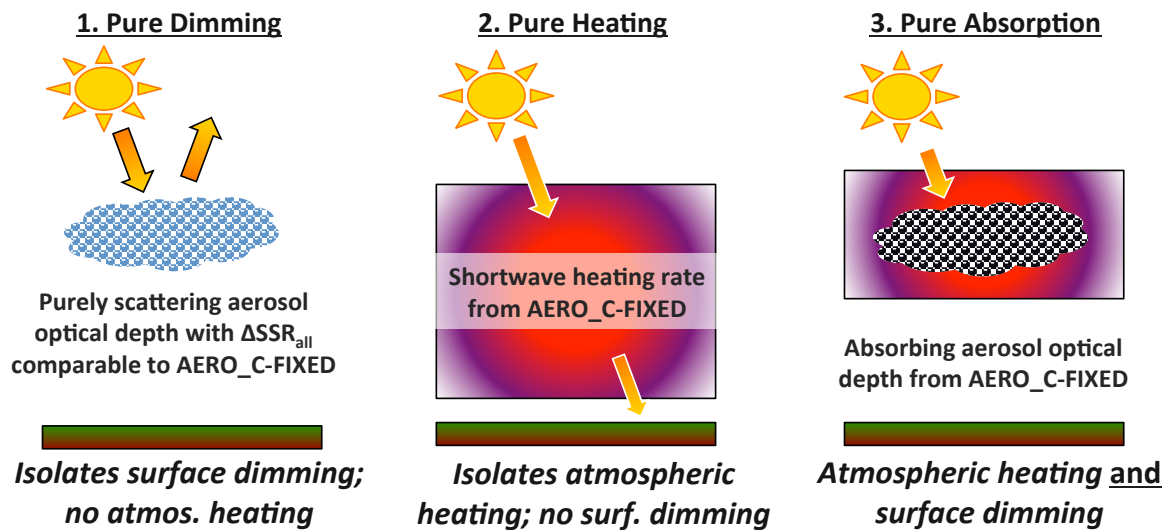
1035 **Fig. 4.** The mid-tropospheric (500 mb) vertical pressure velocity (ω) response (shading; in $10^{-3} \text{ Pa s}^{-1}$)
 1036 to (a) historical regional aerosols, (b) a purely scattering aerosol optical depth, (c) ide-
 1037 alized atmospheric heating, and (d) a purely absorbing aerosol optical depth. Climatological
 1038 values (Pa s^{-1}) are shown in grey contours, and coastal outlines are shown in black. The
 1039 red box delineates East Asia (22.5°–40° N; 100°–122.5° E), over which idealized perturba-
 1040 tions are imposed and regional-means are calculated. Stippling indicates responses that are
 1041 significant at the 95% confidence level. . . . 55

1042 **Fig. 5.** The change in precipitation (shading; in mm day^{-1}) in response to (a) realistic historical
 1043 aerosols (b) a purely scattering aerosol optical depth from historical aerosol, (c) idealized
 1044 atmospheric heating, and (d) a purely absorbing aerosol optical depth. Climatological val-
 1045 ues (in mm day^{-1}) are shown in grey contours, and coastal outlines are shown in black. The
 1046 red box delineates East Asia (22.5°–40° N; 100°–122.5° E), over which idealized perturba-
 1047 tions are imposed and regional-means are calculated. Stippling indicates changes that are
 1048 significant at the 95% confidence level. . . . 56

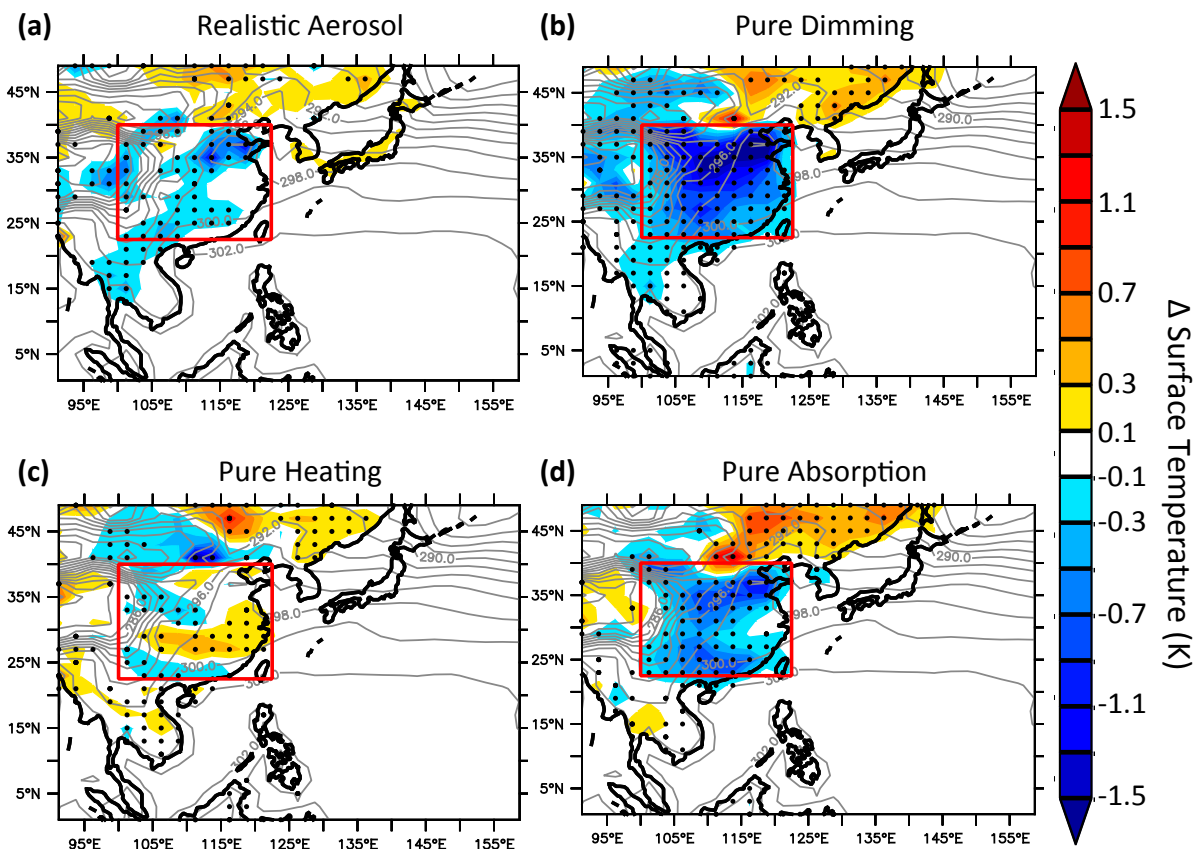
1049 **Fig. 6.** Vertical profiles of changes in (a) pressure velocity (ω) and (b) cloud fraction averaged over
 1050 East Asia (22.5°–40° N; 100°–122.5° E) are shown for the 4 simulations. . . . 57

1051 **Fig. 7.** Vertical profiles of changes in (a) temperature, (b) moisture mixing ratio/specific humidity
 1052 (q), and (c) relative humidity averaged over East Asia (22.5°–40° N; 100°–122.5° E) are
 1053 shown for the 4 simulations. . . . 58

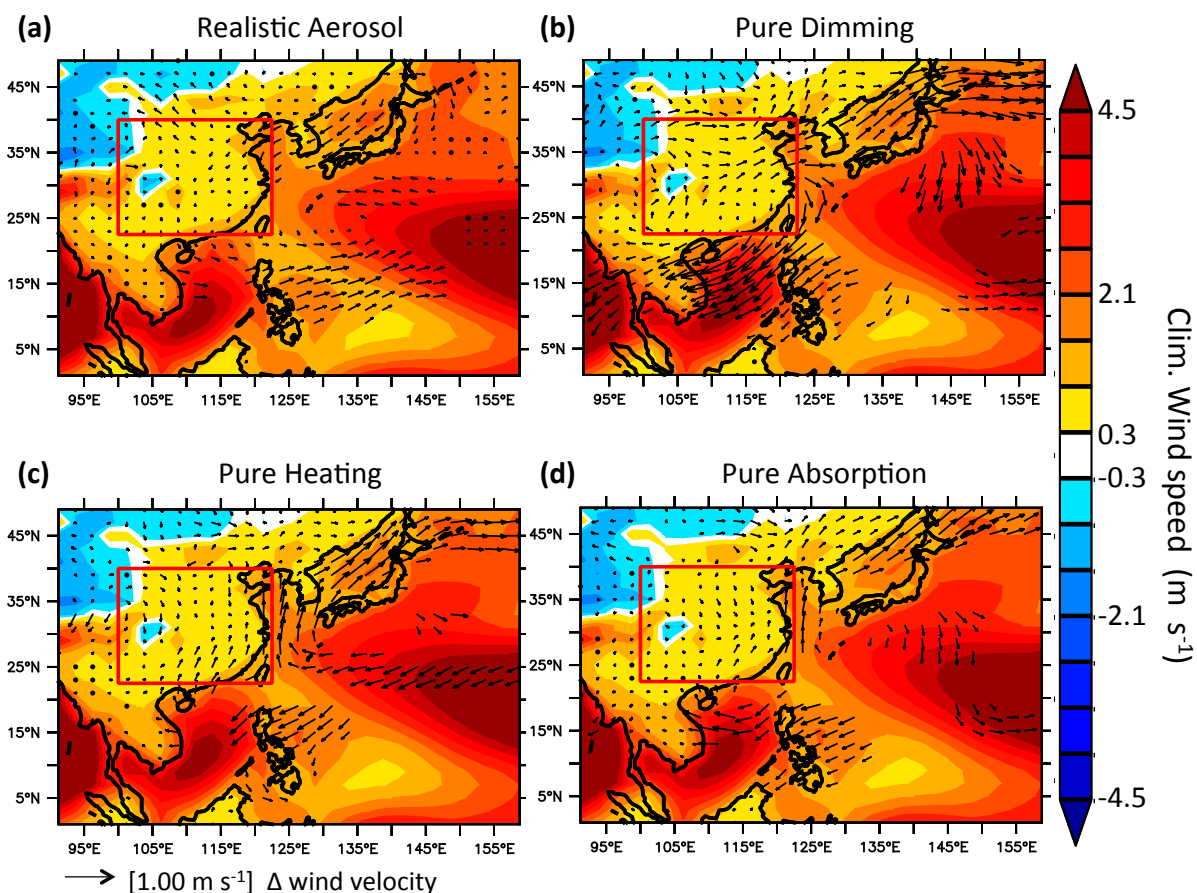
1054 **Fig. 8.** Regional-mean atmospheric heating rates in K day^{-1} are shown for the three idealized forc-
 1055 ing simulations: (a) Pure Dimming, (b) Pure Heating, and (c) Pure Absorption. The heating
 1056 rates due to shortwave radiation (red), longwave radiation (dark blue), latent heat release
 1057 by convective (light blue) and large-scale (black) cloud formation, vertical diffusion (pink),
 1058 and dynamical advection of sensible heat (green; computed as residual of other terms) are
 1059 shown. The shortwave heating rate for the Realistic Aerosol case is also shown (grey) for
 1060 reference in panels (b) and (c). . . . 59



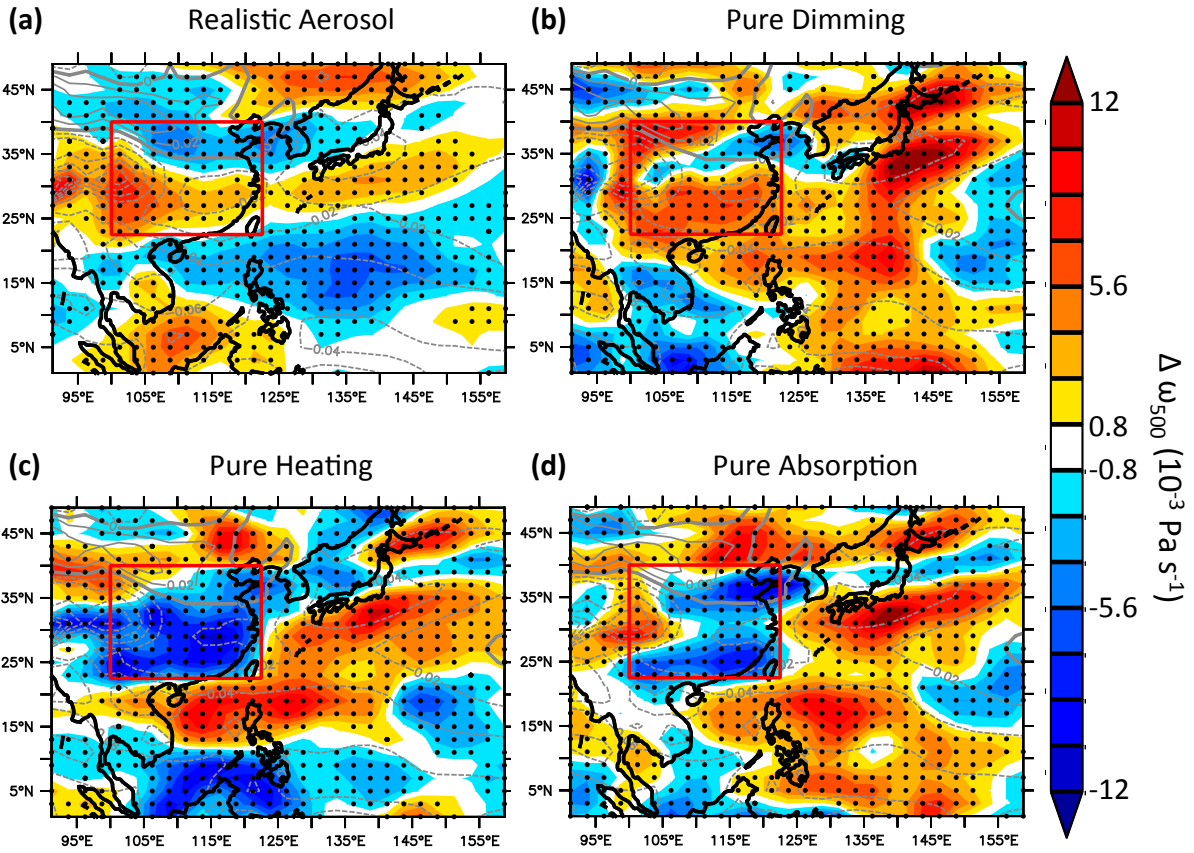
1061 FIG. 1. The 3 idealized forcing perturbations are schematically depicted. Each of the depicted perturbations
 1062 is imposed over Southeast China (22.5°–40° N and 100°–122.5° E) during years 1980–2000 of an ALL con-
 1063 trol simulation, which contains historically varying anthropogenic and natural emissions and observationally
 1064 prescribed sea surface temperature and sea ice.



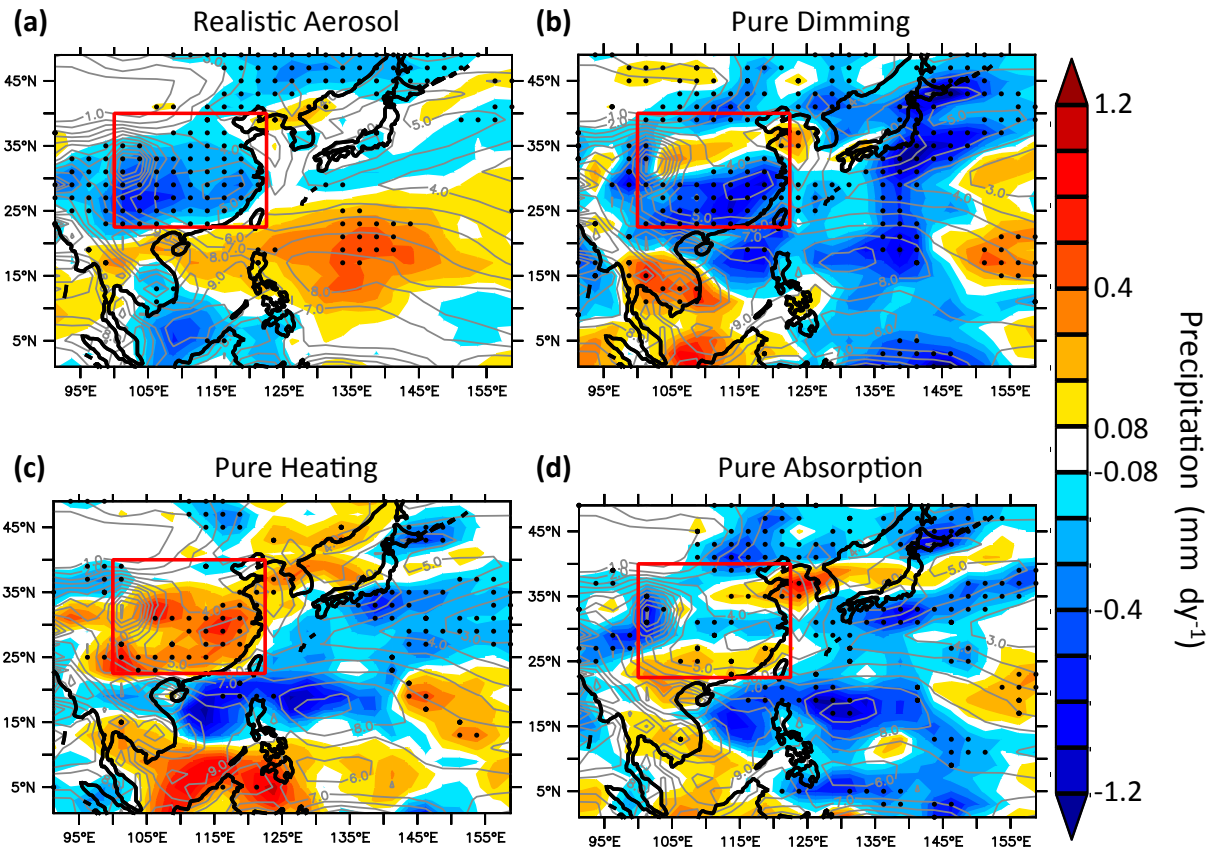
1065 FIG. 2. The surface temperature response (shading; in K) to (a) historical regional aerosols, (b) a purely
 1066 scattering aerosol optical depth, (c) idealized atmospheric heating, and (d) a purely absorbing aerosol optical
 1067 depth. Climatological values are shown in grey contours, and coastal outlines are shown in black. The red
 1068 box delineates East Asia (22.5°–40° N; 100°–122.5° E), over which idealized perturbations are imposed and
 1069 regional-means are calculated. Stippling indicates responses that are significant at the 95% confidence level.



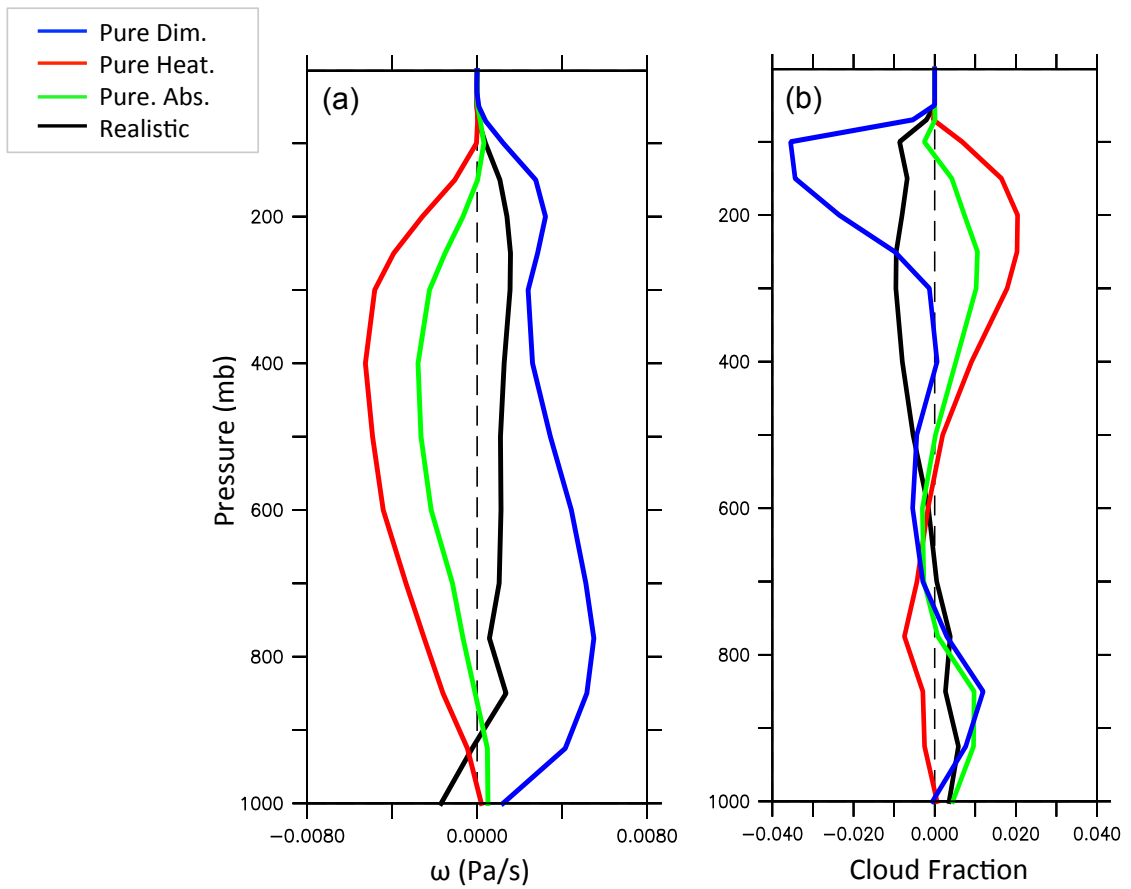
1070 FIG. 3. The change in 850 mb wind velocity (vectors; in m s^{-1}) in response to (a) historical regional aerosols,
 1071 (b) a purely scattering aerosol optical depth, (c) idealized atmospheric heating, and (d) a purely absorbing
 1072 aerosol optical depth. Wind vectors are only shown for changes that are significant at the 95% confidence level.
 1073 Climatological wind speeds (in m s^{-1}) are shaded, with sign convention following meridional wind direction
 1074 (southerly positive). Coastal outlines are shown in black. The red box delineates East Asia (22.5° – 40° N;
 1075 100° – 122.5° E), over which idealized perturbations are imposed and regional-means are calculated.



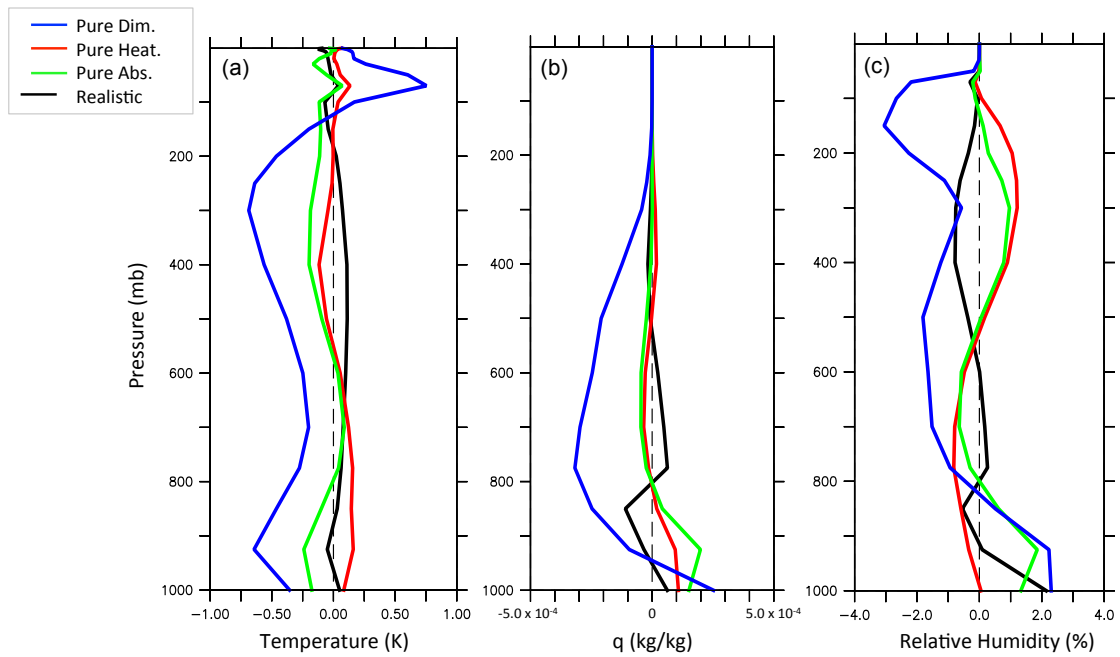
1076 FIG. 4. The mid-tropospheric (500 mb) vertical pressure velocity (ω) response (shading; in $10^{-3} \text{ Pa s}^{-1}$) to
 1077 (a) historical regional aerosols, (b) a purely scattering aerosol optical depth, (c) idealized atmospheric heating,
 1078 and (d) a purely absorbing aerosol optical depth. Climatological values (Pa s^{-1}) are shown in grey contours,
 1079 and coastal outlines are shown in black. The red box delineates East Asia (22.5° – 40° N; 100° – 122.5° E), over
 1080 which idealized perturbations are imposed and regional-means are calculated. Stippling indicates responses that
 1081 are significant at the 95% confidence level.



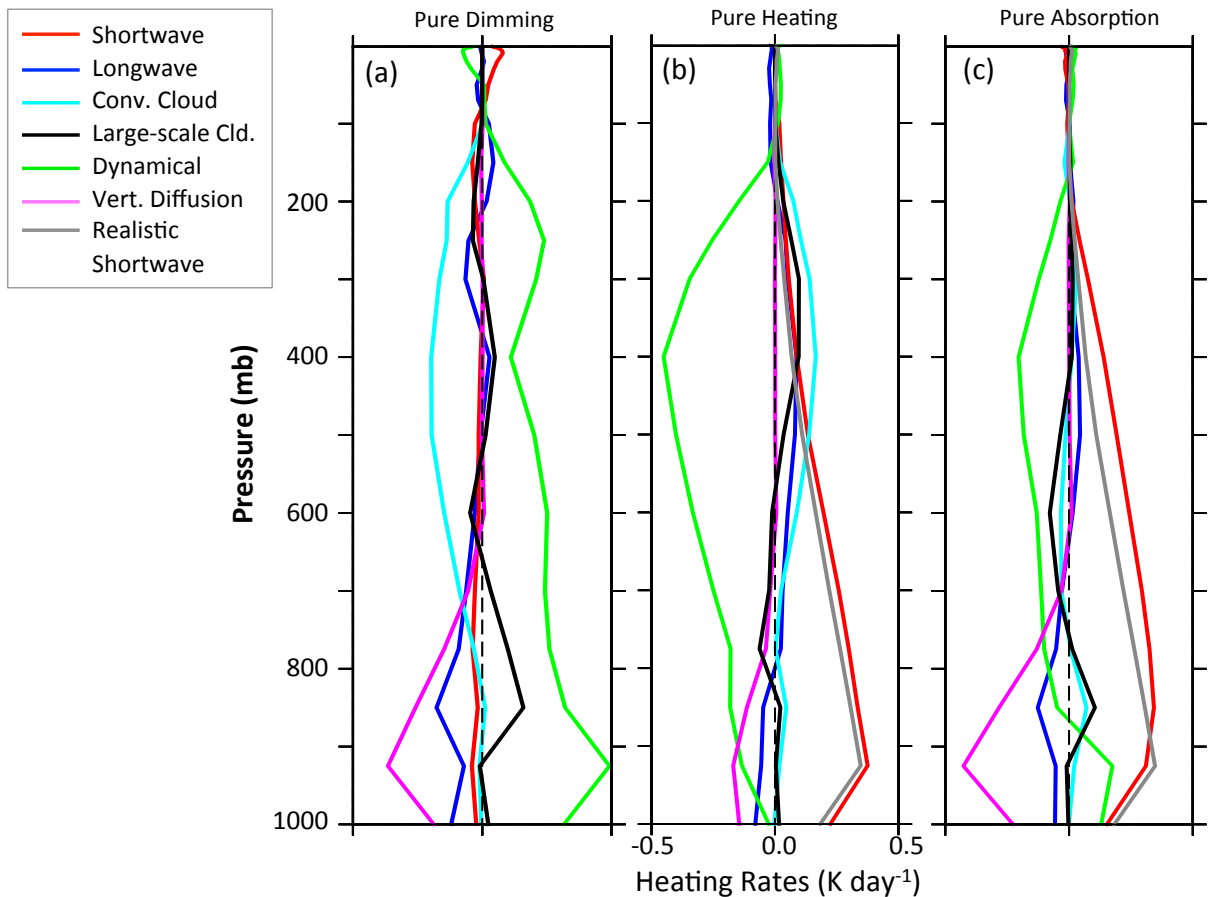
1082 FIG. 5. The change in precipitation (shading; in mm day^{-1}) in response to (a) realistic historical aerosols
 1083 (b) a purely scattering aerosol optical depth from historical aerosol, (c) idealized atmospheric heating, and (d)
 1084 a purely absorbing aerosol optical depth. Climatological values (in mm day^{-1}) are shown in grey contours,
 1085 and coastal outlines are shown in black. The red box delineates East Asia (22.5°–40° N; 100°–122.5° E), over
 1086 which idealized perturbations are imposed and regional-means are calculated. Stippling indicates changes that
 1087 are significant at the 95% confidence level.



1088 FIG. 6. Vertical profiles of changes in (a) pressure velocity (ω) and (b) cloud fraction averaged over East Asia
 1089 (22.5°–40° N; 100°–122.5° E) are shown for the 4 simulations.



1090 FIG. 7. Vertical profiles of changes in **(a)** temperature, **(b)** moisture mixing ratio/specific humidity (q), and
 1091 **(c)** relative humidity averaged over East Asia (22.5°–40° N; 100°–122.5° E) are shown for the 4 simulations.



1092 FIG. 8. Regional-mean atmospheric heating rates in K day^{-1} are shown for the three idealized forcing sim-
 1093 ulations: **(a)** Pure Dimming, **(b)** Pure Heating, and **(c)** Pure Absorption. The heating rates due to shortwave
 1094 radiation (red), longwave radiation (dark blue), latent heat release by convective (light blue) and large-scale
 1095 (black) cloud formation, vertical diffusion (pink), and dynamical advection of sensible heat (green; computed
 1096 as residual of other terms) are shown. The shortwave heating rate for the Realistic Aerosol case is also shown
 1097 (grey) for reference in panels **(b)** and **(c)**.